An *In Vivo* Analysis of the Functional Motifs of DEAD-box RNA Helicase Me31B in *Drosophila* Fertility and Germline Development

Evan Kara[1], Aidan McCambridge[1], Megan Proffer[1], Carol Dilts[1], Brooke Pumnea[1], John Eshak[1], Korey A. Smith[1], Isaac Fielder[1], Dominique A. Doyle[2], Bianca M. Ortega[2], Yousif Mukatash[1], Noor Malik[1], Ammaar R. Mohammed[1], Deep Govani[1], Matthew G. Niepielko[2,3], and Ming Gao[1,*]

1. Biology Department, Indiana University Northwest, Gary, IN, USA

2. School of Integrative Science and Technology, Kean University, Union, NJ, USA

3. Biology Department, Kean University, Union, NJ, USA

***Correspondence**

M. Gao, Biology Department, Marram Hall 310, 3400 Broadway, Gary, IN 46408, USA

Fax: +1 219 980 7125

Tel: +1 219 980 6722

Email: minggao@iun.edu

Abstract

In *Drosophila* germline, Me31B is a putative ATP-dependent, RNA helicase that plays role in post-transcriptional RNA regulation to ensure the correct spatial and temporal

expression of the mRNAs, a process crucial for proper germline development and fertility. However, Me31B's *in vivo* working mechanism remains unclear. In this study, we aim to analyze the functions of Me31B's key domains/motifs to understand how these domains/motifs operate to fulfill the protein's overall activities. We generated *Drosophila* strains mutant for six important motifs including three ATPase/helicase motifs (DEAD-box, DVLARAK, and HRIGR), the N-terminal domain (N-ter), the C-terminal domain (C-ter), and a protein-binding motif (FDF motif-binding motif). In characterizing these mutants, we observed that the three ATPase/helicase motif mutations cause dominant female sterility which is associated with developmental defects in oogenesis and embryogenesis. Follow-up examination of the DVLARAK motif mutant revealed its abnormalities in germline mRNA localization and transcript level. The Me31B N-ter domain (deletion of C-ter), C-ter domain (deletion of N-ter), and mutation of FDF motif-binding motif led to a decrease in female fertility and abnormal subcellular Me31B localizations in the egg chambers. Moreover, deletion of Me31B N-ter or C-ter motif results in a decrease of Me31B protein levels in the ovaries. This study indicates that these six motifs of Me31B play different roles to contribute to Me31B's whole-protein functions like ATPase, RNA helicase, protein stability, protein localization, and partner protein binding, which are crucial for germline development and fertility. Considering Me31B protein family's conserved presence in both *Drosophila* germline and soma (for example, neurons) and in other organisms such as yeast, worm, mouse, and human, the results from this study could expand our understanding of Me31B helicase family's general working mechanisms in different cell types and species.

Introduction

Drosophila Me31B is an evolutionarily conserved, ATP-dependent, DEAD-box RNA helicase that are important for *Drosophila* germline development and fertility [1-5], with homologs like CGH-1 (*C. elegans*) [6, 7], DjCBC-1 (planarians) [8, 9], Xp54 (*Xenopus*) [10, 11], p54 (mouse) [12, 13], and DDX6/Rck (humans) [14-18] playing similar roles in diverse animal species. In these animals, the main role of Me31B family helicases lies in their post-transcriptional RNA regulation including RNA storage, transportation, translational regulation, stabilization, and decay, which ensure the expression of the messages at the correct time and location, and lead to proper germline functioning and development [14, 19-23].

Drosophila Me31B has been employed as a useful model to study the helicases in the family. Me31B's essentiality for *Drosophila* germline has been underscored by that *me31B* loss-of-function mutation or strong knockdown (KD) cause severe egg chamber development defects or early oogenesis arrest, respectively [1, 24]. In normal egg chambers, Me31B proteins express and aggregate into ribonucleoprotein (RNP) complexes, granular assemblies of proteins and RNAs. In these granules, Me31B complexes with other partner proteins like Tral (a translational repressor protein that usually complexes with Me31B in various types of RNP granules) to render post-transcriptional controls on the RNAs within, a process necessary for proper germline development [3, 25-29]. So far, our understanding of Me31B function mostly came from using *Drosophila* strains with complete loss-of-function alleles of *me31B* gene, strains with a significant loss of Me31B proteins, or biochemical analysis of the protein *in vitro*. Therefore, the protein's molecular-level working mechanism *in vivo* remains unclear. In

this study, we aim to analyze the *in vivo* functions of important domains/motifs of Me31B and then understand how they fit together to contribute to Me31B's whole-protein activities.

This study focuses on six Me31B domain/motifs (domains and motifs will be called motifs from here for simplicity): DEAD-box motif (AA 207 – 210), DVLARAK motif (AA 97 – 103), HRIGR motif (381 – 385), N-ter motif (AA 1 – 267), C-ter motif (AA 268 – 459), and FDF motif-binding motif (AA 285 – 289). Previous research suggests that the first three motifs (DEAD-box, DVLARAK, and HRIGR) are crucial for the ATPase/helicase activities of Me31B [30-32]; The two large N-ter and C-ter motifs each contain a RecA-like domain and participate in a wide spectrum of activities including ATPase/helicase, protein binding, and assembly into RNP granules [19, 30, 33]; The FDF motif-binding motif enables Me31B to physically bind to the FDF motifs on translational repressor partners like Tral or EDC3 [33-36]. To study these motifs' *in vivo* functions, we used the CRISPR gene-editing technique and created *Drosophila* strains carrying point mutations that disrupt the motifs' function or deletion mutations in the *me31B* genes (Figure 1). Analysis of the resulting *me31B* mutants revealed that the six motifs are important for *Drosophila* fertility and germline development, while playing different molecular-level roles in localizing germline RNA, maintaining germline RNA level, stabilizing Me31B protein and localizing the protein, and interactions with Me31B partner proteins.

Results and Discussions

Me31B ATPase/helicase motif mutations lead to dominant female sterility.

Although structural and functional studies on Me31B and its homologs identified several ATPase/helicase motifs in Me31B and suggested these motifs' potential functions in ATP hydrolysis, RNA binding, and RNA translational regulation [11, 19, 30, 32, 34, 37, 38], the *in vivo* functions of the motifs have not been investigated. To study this, we introduced single or multiple point mutations to three conserved ATPase/helicase motifs individually: E208A for DEAD box motif (D**E**AD→D**A**AD), R101A and K103A for DVLARAK motif (DVLA**R**A**K**→DVLA**A**AA**A**), and R385Q for HRIGR motif (HRIG**R**→HRIG**Q**). The resulting *me31B* alleles are named $me31B^{E208A}$, $me31B^{DVLAAAA}$, and $me31B^{R385Q}$, respectively (illustrated in Figure 1). The introduced mutations were reported to disrupt the motifs' normal functions in Me31B homologs or structurally similar proteins [30-32, 38-41]. When maintaining the three mutant strains, we immediately noticed that all three alleles dominantly cause female sterility. Specifically, $me31B^{E208A}$/+, $me31B^{DVLAAAA}$/+, and $me31B^{R385Q}$/+ heterozygous female flies do not produce any viable progeny in the presence of males from wildtype w^{1118} strain. In contrast, $me31B^{E208A}$/+, $me31B^{DVLAAAA}$/+, and $me31B^{R385Q}$/+ heterozygous male flies were able to fertilize w^{1118} females and produce viable progenies bearing the mutant *me31B* alleles, suggesting that the three *me31B* alleles cause sterility in females only.

To find out what caused the sterility, we first checked $me31B^{E208A}$/+, $me31B^{DVLAAAA}$/+, and $me31B^{R385Q}$/+ strains for their embryo laying, development, and morphology. Although embryo laying was observed from all three strains, none (0%) of their embryos (n = 541 for $me31B^{E208A}$/+, n = 100 for $me31B^{DVLAAAA}$/+, and n = 17 for $me31B^{R385Q}$/+) were able to develop to larva or later stages on grape agar plates (see Materials and

Methods for the hatchability assay condition). A closer examination of the un-hatched embryos from the three mutants showed that 78% of the embryos from *me31B*^{E208A}/+, 33% of the embryos from *me31B*^{DVLAAAA}/+, and 100% of the embryos from *me31B*^{R385Q}/+ had one or more types of patterning defects like fused dorsal appendages, very short, or no dorsal appendages (Figure 2A), consistent with the strains being sterile. Among the three strains, *me31B*^{R385Q}/+ showed the most severe phenotype: they laid few embryos, and all the embryos laid had severe egg-shell shape defects besides the complete missing of dorsal appendages (Figure 2A).

The embryonic defects in the three mutants indicate that their oogenesis did not proceed normally, so we examined their ovaries. In *me31B*^{E208A} and *me31B*^{DVLAAAA} mutant ovaries, we observed defects in nurse cell dumping, a process in which the nurse cells completely expel all their cytoplasm into late-stage eggs (reviewed in [42]). In the *me31B*^{E208A} mutant, 52% of the stage-14 eggs (n = 13) were still connected with egg chamber tissues that contain nurse cell materials (Figure 2B), indicating incomplete nurse cell dumping. This “dumpless” phenotype is more prominent in *me31B*^{DVLAAAA} mutant: approximately 78% of *me31B*^{DVLAAAA} stage-14 egg chambers (n = 32) did not complete dumping, and the “un-dumped” egg chamber regions were larger than that in the *me31B*^{E208A} mutant (Figure 2C). Consistent with this egg development defect, the *me31B*^{DVLAAAA} mutant showed reduced egg lay when compared to the wildtype control (Supplementary Figure 1). These phenotypes mimic previously reported dumpless phenotypes in the *dcp-1* (encoding a caspase involved in apoptosis) mutant egg chambers, which also lead to decreased egg lay and early embryo development arrest [43]. The *dcp-1* mutation-induced dumpless phenotypes and sterility were associated

with abnormal nucleus envelope breakdown and cytoskeleton organization during nurse cell apoptosis and dumping [43]. Whether the same mechanism is involved in the *me31B*^{E208A} and *me31B*^{DVLAAAA} mutations remains to be analyzed. The most severe oogenesis defects were observed in the *me31B*^{R385Q} mutant, as we observed frequent egg chamber degenerations at early-to-mid stages (Figure 2D), consistent with this mutant's few egg lay and sterility.

The sterility and defects in oogenesis and embryogenesis in all three mutants suggests that each ATPase/helicase motif is needed for *Drosophila* germline growth, and their cooperative actions are likely needed to output the correct ATPase/helicase function. An explanation for these mutations being dominant could be that the mutations introduced detrimental functions that leads to the mutant Me31B protein being "toxic" to germline cells. This explanation is supported by previous research on similar mutations made in other RNA helicases. For example, in eIF4A, another DEAD-box RNA helicase important for germline mRNA translational control [44, 45], D**E**AD→D**Q**AD and HRIG**R**→HRIG**Q** mutations cause the protein to become dominant negative in translation *in vitro* [46-48]. As another example, in an assay of Xp54 (Me31B homolog in *Xenopus*)'s effect on tethered RNAs, D**E**AD→D**Q**AD mutation, DILA**R**A**K** (homologous to DVLARAK in Me31B)→DILA**A**A**A** mutation, and HRIG**R**→HRIG**Q** mutations changed the protein's regulation on substrate RNAs from translational repression to translational activation [30]. These reports made us postulate that the dominant sterility effects of *me31B*^{E208A}, *me31B*^{DVLAAAA}, and *me31B*^{R385Q} mutations may be caused by altered RNA translational control activity of the mutated proteins.

It is integral to note that the HRIG**R**→HRIG**Q** mutation caused much more severe germline phenotypes than the D**E**AD→D**A**AD or DVLA**R**A**K**→DVLA**A**A**A** mutations. We suspect this may be either that 1) substituting an ATPase/helicase motif's key amino acid (like arginine, R) to glutamine (Q) causes more detrimental effects than alanine (A), or that 2) the HRIGR motif plays a separate and more important roles than the DEAD and DVLARAK motifs. Previous research in other systems provided conceptual support for both explanations. For the first argument, D**Q**AD mutation in the DEAD-box motif of GLH-1 (a conserved germ granule RNA helicase in *C. elegans*) led to a more severe fertility decrease and embryo arrest phenotypes than D**A**AD mutation [49, 50]. For the second, D**E**AD→D**Q**AD mutation in the DEAD-box helicase eIF4A abolish the protein's ATPase activity but retain a small amount of RNA-binding activity, while the HRIG**R**→HRIG**Q** mutation abolishes RNA-binding ability but retains some ATPase activity [46], suggests that the HRIGR motif may perform unique steps/roles in the helicase's enzymatic actions.

Me31B helicase activity functions in *nos* localization by modulating *osk* and *nos* transcript levels

Considering Me31B's known role in post-transcriptional RNA regulation on important germline mRNAs such as *nanos* (*nos*), we investigated whether the above ATPase/helicase mutations affect *nos* localization to its germ plasm destination in late-stage eggs (germ plasm is a special cytoplasm at the posterior pole of late-stage eggs and early embryos; germ plasm contains mRNAs needed for processes including embryo patterning and germ cell formation. For reviews, see [51-55]). Normal *nos*

localization occurs through the Oskar-dependent formation of homotypic clusters within germ granules, aggregates that contain multiple copies of *nos* transcripts [56, 57]. We tested this hypothesis with the *me31B*^{DVLAAAA}/+ strain and performed single molecule fluorescent *in situ* hybridization (smFISH) on stage 13 oocytes to identify both unlocalized *nos* transcripts and *nos* clusters in the posterior germ plasm. Using previously established imaging and image analysis techniques [56, 57] (See Material and Methods), we quantified the number of *nos* transcripts that reside within homotypic clusters in the *me31B*^{DVLAAAA} mutant and a control CRISPR strain (*me31B*^{WT}*-GFP*) with wildtype *me31B* gene (Figure 3A). We found that the average number of *nos* transcripts found in a homotypic cluster of the control was 6.42 ± 0.47 transcripts per cluster which were not significantly different from the previously published average of 7.58 ± 0.42 transcript per *nos* cluster in *yellow white* flies ($p = 0.12$) [57], suggesting that our CRISPR genome modifications like adding the GFP tag does not affect *nos* localization. However, in the *me31B*^{DVLAAAA} mutant, the average number of *nos* transcripts found in a homotypic cluster is 2.33 ± 0.21, a significant reduction when compared to the *me31B*^{WT}*-GFP* control ($p < 0.0001$). Together, these data suggest that the Me31B helicase activity influences *nos* localization to the posterior germ plasm.

We next explored the mechanisms by which Me31B influences *nos* localization. Recently, it has been shown using computational modeling and experimental validation that the localization of *nos* is influenced by 1) the number of *nos* transcripts that are expressed, 2) the amount of Osk in the system, and 3) *nos*'s clustering factor, a quantifiable effect that, in conjunction with transcript and Osk levels, regulates the number of transcripts that can accumulate within a homotypic cluster [57, 58]. To

identify whether *me31B*^{DVLAAAA} affects one or more of these mechanisms, we first conducted RT-PCR to measure the level of *nos* and *osk* RNAs in the system. We found that *nos* transcript levels were reduced to 61% ± 7% of wild-type levels and *osk* levels were reduced to 56% ± 4% when compared to wild-type ($p < 0.05$) (Figure 3C). To determine whether these changes can account for the observed reduction of *nos* homotypic cluster sizes in the *me31B*^{DVLAAAA} mutant, we used computational modeling to recapitulate *nos* localization *in silico* by adjusting a previously published model's parameters [58] from 1.00 to 0.61 for *nos* transcript levels and from 1.00 to 0.56 for Osk levels (See Material and methods). Modeled *nos* homotypic clusters contained an average of 2.86 transcripts per cluster which was not significantly different from the average produced by the *me31B*^{DVLAAAA} mutant ($p = 0.988$) (Figure 3B). Together, these data suggest that the mechanism creating the *nos* localization defect in *me31B*^{DVLAAAA} mutant is caused by a combined effect generated by the reduction of *nos* and *osk* levels.

Me31B is a known component of an ATP-dependent assembly of a stable, repressed ribonucleoprotein particle (RNP) containing *nos* [3, 22]. In the *me31B*^{DVLAAAA} mutant, ATP-dependent helicase activity is presumably disrupted, causing a reduction of *nos* transcripts (Figure 3C). Combining our new data with previous findings that Me31B functions in post-transcriptional mRNA regulation like RNA stability control [1-3, 28, 36], we suggest that Me31B functions in stabilizing unlocalized RNPs containing *nos* and *osk*, allowing for stable mRNAs to reach and become incorporated into the germ plasm. Furthermore, we suggest that disruption of DVLAAAA motif results in a destabilization of mRNAs that have not localized to the germ plasm, resulting in a decrease in *nos* and

226 *osk* that are available to form the germ plasm and ultimately reducing the *nos*
227 localization. Additional germ plasm mRNAs such as *cycB*, *pgc*, and *gcl* also diffuse to
228 the posterior RNPs containing a single transcript and form homotypic clusters within
229 germ granules [56]. Thus, future studies should explore whether Me31B's helicase
230 activity is specific to *nos* or has a more global role in stabilizing unlocalized germ plasm
231 mRNAs. To find out whether *nos* and *osk* transcripts level changes also occur in the
232 other two ATPase/helicase mutants ($me31B^{E208A}$/+ and $me31B^{R385Q}$/+), we measured
233 the transcript levels of the two RNAs in the two mutants. To our surprise, in
234 $me31B^{E208A}$/+ flies, *nos* level remains comparable (104% ± 7%) to w^{1118} control strain,
235 while *osk* mRNA level is significantly up-regulated (162% ± 12%) (Figure 3D). In
236 $me31B^{R385Q}$/+ flies, *nos* mRNA showed a significant decrease (44% ± 2%), while *osk*
237 level showed a significant increase (194% ± 12%) when compared to the control (Figure
238 3E). Comparing the changes of nos and osk between the three ATPase/helicase
239 mutants, (compare Figure 3C, D, and E), we found that the three dominant-sterile
240 mutations caused nonuniform effects on the levels of *nos* and *osk*. This suggests that
241 the three motifs play different roles in maintain germline mRNA levels or they are
242 responsible for maintaining different RNAs. From this, we further suggest that the
243 change of *nos* and *osk* levels cannot be the only cause for the sterility of the three
244 mutants. Further studies are needed to reveal and contrast how different
245 ATPase/helicase motif mutations globally affects germline RNAs.
246

Me31B N-ter motif, C-ter motif, and FDF motif-binding motif mutations decrease female fertility

We next analyzed the functions the Me31B N-ter motif (amino acids 1 – 267), C-ter motif (amino acids 268 – 459), and FDF motif-binding motif (amino acids 285 – 289). The N-ter motif contains a RecA-like domain and contributes to the protein's ATP binding, helicase activity, and P-body assembly ability [19, 30]. The C-ter motif also contains a RecA-like domain and contributes to the protein's ATP hydrolysis, helicase activity, RNA translational repression, partner-protein binding, and P-body assembly ability [30, 33, 35, 59]. The FDF motif-binding motif allows Me31B to physically interact with FDF motifs in partner RNA repressor proteins like Tral and EDC3 [3, 4, 28, 33, 34, 36]. To study these motifs' contributions to Me31B whole-protein activities, we generated *me31B*$^{N\text{-}ter}$, *me31B*$^{C\text{-}ter}$, *me31B*^{FDF}, and *me31B*^{WT} alleles which contain the N-ter coding sequence, the C-ter coding sequence, point mutations in FDF motif-binding motif, and wildtype *me31B* gene (as control), respectively (illustrated in Figure 1). We do note that our attempts to generate the original N-ter (AA 1 - 267) and C-ter (AA 268 - 459) mutations were hindered by technical difficulties, but we were able to generate N-ter (AA 1 - 276) and C-ter (AA 277 - 459) mutations instead, so the latter constructs were used in this study. We first screened the mutants homozygous for the three alleles (*me31B*$^{N\text{-}ter}$, *me31B*$^{C\text{-}ter}$, and *me31B*^{FDF}) for their fertility by using a previously reported female fertility assay [60]. In this assay, the egg laying and progeny production (hatchability) were separately analyzed to yield a more complete understanding of how the fertility were affected in these mutants. The assay showed that *me31B*$^{N\text{-}ter}$, *me31B*$^{C\text{-}ter}$, and *me31B*^{FDF} mutant females showed a significant fertility decrease when

compared to the *me31B*^{WT} control (Figure 4A). Specifically, in the egg laying part, a *me31B*^{WT} control female fly laid an average of 117 eggs during the assay period, while a *me31B*$^{N\text{-}ter}$, *me31B*$^{C\text{-}ter}$, and *me31B*^{FDF} fly laid an average of 68, 29, and 77 eggs, respectively, a significant decrease of 42.9%, 75.2%, and 34.2%, respectively (Figure 4A). In the progeny production part, a *me31B*^{WT} control female produced an average of 106 progeny flies, while a *me31B*$^{N\text{-}ter}$, *me31B*$^{C\text{-}ter}$, and *me31B*^{FDF} fly produced 47, 0, and 75 progenies, a significant decrease of 55.7 % and 100% and an insignificant decrease of 29.2%, respectively (Figure 4B). The obvious absence of progenies from the *me31B*$^{C\text{-}ter}$ mutant indicated that the *me31B*$^{C\text{-}ter}$ females were sterile. To validate this, we collected the eggs (n = 97) from *me31B*$^{C\text{-}ter}$ females (accompanied by *w*^{1118} males) on grape-juice agar plates and examined the eggs' development. We observed that none of the eggs developed to larva or later stages and that all the eggs showed morphological defects including fused dorsal appendages (n = 66, 68% off the eggs) or no dorsal appendages (n = 31, 32% of the eggs) (Figure 4D), consistent with *me31B*$^{C\text{-}ter}$ females being sterile.

We calculated the egg hatchability rate of the three mutants by dividing the number of viable progenies by the number of eggs laid. The hatchability rates of *me31B*$^{N\text{-}ter}$ and *me31B*$^{C\text{-}ter}$ strains are 68.3% and 0%, respectively, a significant decrease when compared to the control's 90.8% hatchability rate (Figure 4C). For the *me31B*^{FDF} strain, the hatchability (97.1%) is not significantly different from the control (Figure 4C).

We conclude that Me31B's N-ter or C-ter motifs (when expressed alone) and mutation in the FDF motif-binding motif cause *Drosophila* female fertility decrease. Particularly, *me31B*$^{N\text{-}ter}$ mutant and *me31B*$^{C\text{-}ter}$ mutant cause defects in both egg-lay quantity and

egg hatchability. However, we cannot neglect that the sterility of *me31B*$^{C\text{-}ter}$ mutant is a stronger fertility defect than the *me31B*$^{N\text{-}ter}$ mutant, suggesting the two domains' different importance in maintaining fertility. Considering that *me31B* is an essential gene and its loss-of-function mutations are lethal [1], we were surprised to see that either Me31B N-ter or C-ter motif (when expressed alone) is enough to support fly viability, suggesting that either motif is able to provide certain essential, full-length-protein functions that enables *Drosophila* growth. Comparatively, *me31B*^{FDF} strain showed the smallest fertility decrease with no measurable defects in egg hatchability. This means that the disruption of Me31B's FDF-motif binding function has only a mild negative effect on fertility.

Me31B N-ter motif, C-ter motif mutations decrease Me31B protein level.

To follow up with the fertility defects in the *me31B*$^{N\text{-}ter}$, *me31B*$^{C\text{-}ter}$, and *me31B*^{FDF} mutants, we hypothesize that these mutations may have changed Me31B protein stability and therefore reduced the amount of protein in the germline. To test this, we took advantage of the GFP-tags fused to the wildtype and mutant Me31B proteins and used anti-GFP Western blots to quantify the proteins in the ovaries of the mutant strains. We observed that the Me31B$^{N\text{-}ter}$ and Me31B$^{C\text{-}ter}$ protein levels are 40% and 11% of the Me31B^{WT} control, respectively (Figure 5A and 5B). The Me31B^{FDF} protein level (114%) is comparable to the Me31B^{WT} control. We conclude that the N-ter and C-ter motifs are important for maintaining Me31B protein level and deleting either half of the protein likely destabilized the protein. We also suggest that the Me31B$^{C\text{-}ter}$ protein (N-terminal deletion) is even less stable than the Me31B$^{N\text{-}ter}$ protein (C-terminal

316 deletion). Together with the fertility experiments (Figure 4), we noticed that the mutant
317 strains' fertility and their mutant protein expression level share a similar trend, with
318 *me31B*$^{C\text{-}ter}$ mutant showing complete sterility and the least level of protein expression
319 and *me31B*^{FDF} mutant showing a mild fertility decrease and near wildtype-level protein
320 expression (compare Figure 4 and Figure 5B). We speculate that, besides the likely
321 altered Me31B protein functions, the change of protein abundance could also be a
322 factor that decreased the fertility of the mutants.
323

324 **Me31B N-ter motif, C-ter motif, and FDF motif-binding motif mutations alter**
325 **Me31B subcellular localization**
326 Me31B is abundantly expressed in the cytoplasm of nurse cells and developing oocytes
327 in *Drosophila* ovaries. In these cells, Me31B complexes with partner protein Tral and
328 aggregate together into RNP granules including perinuclear granules (nuage granules)
329 in nurse cells, P-body/sponge body granules in nurse cells and oocytes, and germ
330 plasm granules in oocytes [1, 24, 28]. To find out whether the *me31B*$^{N\text{-}ter}$, *me31B*$^{C\text{-}ter}$,
331 and *me31B*^{FDF} mutations affect Me31B subcellular localization, we used the GFP-tags
332 on the Me31B proteins to visualize them in the ovary cells and used anti-Tral
333 immunostaining to mark the germline RNP granules.

334 In the early-stage egg chambers (Figure 6A), wildtype Me31B^{WT}-GFP and Tral both
335 localize to the nuage granules and the P body/sponge body granules in the nurse cells
336 and developing oocytes (Figure 6A, first row). The two proteins showed extensive
337 overlap at these granules, suggesting likely colocalization. This localization pattern of
338 Me31B^{WT}-GFP and Tral is indistinguishable from the wildtype proteins in Oregon-R

339 strains or GFP-Trap strains carrying wildtype *me31B* genes [1, 24]. However, in
340 *me31B*$^{N\text{-}ter}$, *me31B*$^{C\text{-}ter}$, *me31B*^{FDF} egg chambers, the three mutant Me31B-GFP proteins
341 were conspicuously more diffused in the nurse cells and oocytes, and they no longer
342 overlap with Tral whose localization remain similar to that in the *me31B*^{WT} control
343 (Figure 6A, 3 bottom rows). This indicates that Me31B N-ter motif, C-ter motif, and the
344 FDF motif-binding motif are needed for Me31B's aggregation status. Furthermore, the
345 three mutant proteins each showed distinct localization/distribution patterns. Me31B$^{N\text{-}ter}$-
346 GFP proteins are found in the nurse cell nucleus (Figure 6A, second row), which is
347 further confirmed by co-staining the egg chambers with DNA stain DAPI
348 (Supplementary Figure 3). Although a small number of Me31B$^{C\text{-}ter}$-GFP aggregates
349 were observed (Figure 6A, third row), they are fewer and smaller than Me31B^{WT}-GFP
350 aggregates. From these observations, we conclude that Me31B's proper aggregation
351 into germline RNP granules requires the presence of both the N-ter motif and C-ter
352 motif. Previous studies suggest that the two motifs contain different sequence
353 components and therefore different potential functions. The N-ter motif contains several
354 ATPase/helicase motifs including DEAD-box motif and DVLAAAA motif but no known
355 protein-binding motifs [30-32, 35]; The C-ter motif contains several protein-binding
356 motifs and one putative helicase motif, HRIGR) [10, 19, 30, 33, 35, 59]. This means that
357 Me31B likely uses it RNA-interaction ability on both N-ter and C-ter motifs and the
358 protein-binding ability on the C-ter motif to aggregate into the RNP granules. In line with
359 this speculation, the failure of Me31B^{FDF}-GFP to aggregate (Figure 6A, bottom row)
360 suggests that interaction/recruitment by FDF-motif proteins like Tral and EDC3 [34, 61]
361 is necessary for Me31B's aggregation process. We note that Me31B^{FDF}-GFP's failure to

aggregate is independent of its protein expression level (Figure 5). Together with the mild fertility decrease of the *me31B*^{FDF} strain (Figure 4), we suggest that Me31B's aggregation status per se only has a small influence on *Drosophila* fertility. Another aggregation factor in Me31B protein is the two predicted Intrinsically Disordered Regions (IDRs) at the N-ter end (AA 1- 53) and the C-ter ends (AA 431 – 459), respectively. Deleting the IDRs caused rapid self-assembly of Me31B into aggregate-like structures *in vitro*, so the IDRs were suggested to attenuate the interactions between the folded N-ter and C-ter motifs [62]. From the above pieces of evidence, Me31B aggregation to germline RNP granule could be a complex interplay between RNA-interacting, partner protein binding, and IDRs.

About the confounding nuclear localization of Me31B$^{N\text{-}ter}$ proteins, we speculate that Me31B may be a nucleocytoplasmic shuttling protein with a Nuclear Localization Signal (NLS) sequence in the N-terminal motif. This NLS sequence leads Me31B into the nucleus, and then the C-terminal motif mediates the protein's export and retaining in the cytoplasm. This speculation is conceptually supported by the nucleocytoplasmic shuttling activities of DDX6 (human homolog of Me31B) [59] and Xp54 (*Xenopus* homolog) [11] in cell culture models. However, our efforts to identify a Nuclear Localization Signal (NLS) sequence by using prediction tools (NLStradamus [63], cNLS Mapper [64], and SeqNLS Prediction Server [65]) were unsuccessful. Although we were able to locate amino acid sequences in Me31B (KSKLKLPPKDNRFK and CIPVLEQIDP) that are homologous to the putative NLS and Nuclear Export Signals (NES) sequences in DDX6 [59] respectively, experimental evidence is still needed to validate their *in vivo* functionality. We do not exclude the possibility that the N-terminal

385 NLS is just a non-functional sequence that is normally masked in folded, full-length
386 Me31B protein, and the sequence was accidentally exposed to nucleus transportation
387 machinery upon the deletion of the C-terminal motif.

388 In the early-to-mid stage egg chambers (Figure 6B), we observed that Me31B
389 enrichment in developing oocytes is abolished in the three mutants. In the *me31B*^{WT}
390 control egg chambers, Me31B^{WT}-GFP and Tral both were highly enriched in the
391 developing oocytes, with the two proteins extensively overlapping (Figure 6B, first row).
392 However, in the *me31B*$^{N\text{-}ter}$ and *me31B*$^{C\text{-}ter}$ egg chambers, the mutant Me31B proteins
393 show no obvious enrichment in the future oocytes (Figure 6B, second and third row),
394 while Tral's enrichment pattern remain unaffected. In the *me31B*^{FDF} mutants, the
395 Me31B^{FDF}-GFP proteins still showed enrichment in the oocytes, but it is much weaker
396 than the Me31B^{WT}-GFP control. We conclude that the Me31B N-ter motif, C-ter motif,
397 and the FDF motif-binding motif are needed for the protein's proper accumulation into
398 future oocytes at early-to-mid stages. For similar reasons discussed before, we suggest
399 that Me31B's transport/accumulation into the oocytes depends on its RNA-interaction
400 and protein-binding abilities. This speculation is in line with the observation that
401 Me31B^{FDF} proteins maintained a reduced enrichment in the oocytes: the protein's intact
402 RNA-interacting motifs or other protein-binding motifs could have enabled an ineffective
403 but functional transportation into the oocytes.

404 In the mid-stage egg chambers (Figure 6C), Me31B^{WT} proteins were found along the
405 cortex and localized to the germ plasm area of the oocytes (Figure 6C, first row), similar
406 to the Me31B proteins in wildtype strains as previously reported [28]. In the *me31B*$^{N\text{-}ter}$,
407 *me31B*$^{C\text{-}ter}$, *me31B*^{FDF} mutants, the three mutant proteins localized to the above areas,

but the localized proteins appeared to have less granularity (Figure 6C, bottom three rows), consistent with the diffused status of the mutant proteins in earlier stages.

To further validate that the above localization phenotypes of the mutant Me31B proteins were not a result of defective germline RNP formation, we performed immunostaining against another germline RNP marker, Cup, a protein that complexes with both Me31B and Tral in germline RNPs such as nuage granules, P-body granules, and germplasm granules [28]. We found that, like Tral, Cup's aggregation and localization into those RNPs remain unchanged in the *me31B* mutants (data not shown).

Summary

All in all, this study took a mutagenesis approach to investigate the *in vivo* functions of six key motifs of DEAD-box RNA helicase Me31B, and the results are summarized in Figure 7. The three ATPase/helicase motifs (DEAD-box, DVLARAK, and HRIGR) are conserved among the members of the Me31B protein family, and mutations in each of them result in alleles (*me31B*^{E208A}, *me31B*^{DVLAAAA}, and *me31B*^{R385Q}) that cause dominant female sterility. Their sterility exhibits oogenesis defects like nurse cell dumping defects or egg chamber degeneration and early embryogenesis arrest accompanied by embryo morphological abnormalities. In our attempt to find the molecular-level mechanism by which the ATPase/helicase motif mutations cause sterility, we analyzed the *me31B*^{DVLAAAA} heterozygous mutant and showed that the mutation altered *nos* mRNA localization in the germ plasm and decreased *nos* and *osk* transcript levels, highlighting Me31B ATPase/helicase's function in maintaining germline mRNA localization and transcript level. Our additional analysis of Me31B's N-ter motif, C-ter motif, and FDF motif-binding motif demonstrated their impotence in fertility,

maintaining Me31B protein level and aggregation status, and subcellular localization. The results from this study provided insight on the molecular mechanisms of key functional motifs in *Drosophila* Me31B. Considering the conserved nature of Me31B and its homologs, these data aid in paving the road to understanding the functions and important regions of Me31B family proteins in various cell types and across different species.

Materials and Methods

Fly strain generation by CRISPR gene editing

Mutant *me31B Drosophila* strains were generated by using the previously reported CRISPR procedure [66, 67]. Specifically, CRISPR Optimal Target Finder [66] and DRSC/TRiP Functional Genomics Resources (Harvard Medical School) were used to find gRNA cutting sites flanking the *me31B* gene in the *Drosophila* genome. Then, the found gRNA sequences were cloned into gRNA-expressing plasmid vector pCFD5 (Addgene) according to the suggested protocols. HDR donor plasmids carrying wild type *me31B* gene were constructed by cloning *me31B* gene DNA into pHD-sfGFP-ScarlessDsRed cloning vector (Addgene) according to suggested protocols. In the constructed HDR plasmids, the super-fold GFP (*sfGFP*) gene is positioned in-frame and downstream of the *me31B* gene so that the sfGFP protein is tagged to the C-terminal end of the expressed Me31B proteins. The *DsRed* marker gene is positioned in the intergenic region downstream of the *me31B* gene. HDR plasmid with mutant *me31B* genes was generated by mutating the *me31B* wild type gene in the wildtype HDR donor plasmid by using the Site-Directed Mutagenesis kit (New England Biolabs) according to

454 the manufacturer's recommended protocols. The resulting HDR plasmids containing
455 different *me31B* alleles are named after the carried mutations (Figure 1). The gRNA-
456 expressing plasmid and the HDR donor plasmids were co-injected into Cas9-expressing
457 strain (Genetivision) to generate desired wild type and *mutant* me31B strains, which
458 were crossed with a 2nd chromosome balancer to establish balanced stocks when
459 possible. The plasmid vectors constructed and the obtained *me31B* strains were
460 validated by sequencing.

461 **Genetic crosses**

462 Balanced *me31B* wild type and mutant strains were self-crossed to obtain homozygous
463 mutant strains. For the dominant female sterile *me31B* strains, males carrying the
464 mutant allele were crossed with w^{1118} (Bloomington Drosophila Stock Center 3605)
465 females to obtain heterozygous strains.

466 **Immunohistochemistry**

467 *Drosophila* ovary immunostaining was performed as previously described [24, 68, 69].
468 The following antibody dilutions were used: Rabbit-anti-Tral (1:1,000). Donkey-anti-
469 Rabbit-Cy3 secondary antibodies (Jackson ImmunoResearch) were used at 1:500.
470 Images were captured by an Olympus FV3000 confocal laser scanning microscope.

471 **Western blots**

472 Western blot antibodies were used at the following dilutions: rabbit-anti-GFP
473 (1:100,000), and mouse-anti-α-Tubulin (1:100,000). Secondary antibodies were used at
474 the following dilutions: mouse-anti-rabbit HRP (Jackson ImmunoResearch) (1:10,000 for
475 rabbit-anti-GFP), goat-anti-mouse HRP (Santa Cruz Biotechnology) (1: 50,000 for

476 mouse-anti-α-Tubulin primary antibody). The protein band quantification analysis was
477 performed by using ImageJ (https://imagej.nih.gov/ij/)

478 **Fertility assay (for *me31B^{WT}*, *me31B$^{N\text{-}ter}$*, *me31B$^{C\text{-}ter}$*, and *me31B^{FDF}* strains)**
479 Fertility assays were performed according to previously established protocols [60].
480 Briefly, virgin females from *me31B^{WT}*, *me31B$^{N\text{-}ter}$*, *me31B$^{C\text{-}ter}$*, and *me31B^{FDF}* strains
481 were collected and allowed to age for 3 – 4 days separately in fly food vials. Each
482 female was then put in a vial in with a *w^{1118}* male. After 24 hours, the males were
483 removed from the vials, the fertilized females were transferred to a new vial every day
484 for the next 10 days. The eggs laid and the progenies hatched from each vial were
485 counted. The hatch rate of each vial is calculated by dividing the progenies hatched by
486 the number of eggs laid. An equal amount (15 ml) of fly food medium (Molasses
487 Formulation, Genesee Scientific) was used in each vial.

488 **Number of egg laying, embryo morphology, and embryo hatchability (*me31B^{E208A}*,**
489 ***me31B^{DVLAAAA}*, and *me31B^{R385Q}* strains)**
490 To record the number of eggs laid from *me31B^{DVLAAAA}*/+ strain, 40 females from the
491 strain were put into a small embryo collection cage with grape-agar plates
492 (Genetivision) in the presence of 10 *w^{1118}* males. After letting the flies adjust for 24
493 hours, the flies were given a fresh grape agar plate, and the eggs laid in the next 24
494 hours were counted. Control experiments were conducted with *w^{1118}* females, and six
495 independent replicates were performed. To observe the morphology and the hatchability
496 of the embryos from *me31B^{E208A}*/+, *me31B^{DVLAAAA}*/+, *me31B^{R385Q}*/+, and *w^{1118}* control
497 strains, approximately 80 females from each strain were put into a small embryo
498 collection cage in the presence of 20 *w^{1118}* males, and the embryos were collected on

grape agar plates at 25ºC after 24 hours. The embryos were counted and analyzed under a dissection microscope for their morphology. The embryos' hatchability was calculated 72 hours after they were laid by counting the number of those that developed into larvae (or later stages) or by counting those that failed to develop and then subtracting the failed ones from the total number of eggs laid.

RNA extraction, cDNA synthesis, and quantitative RT-PCR

Ovarian total RNA was extracted from 5 µl freshly dissected fly ovaries by using Qiagen RNeasy Purification Kit (Qiagen) according to the manufacturer's instructions. The obtained RNA samples' concentrations were measured by using NanoDrop 2000c. The RNAs were reversely transcribed to cDNAs by using the High-Capacity cDNA Reverse Transcription Kit (ThermoFisher) according to the manufacturer's instructions. The synthesized cDNAs were then used for quantitative PCR by using Luna Universal qPCR Master Mix (New England Biolabs). The following PCR Primers were used in this study: *nos* forward 5' GTCACCAGCAAACGGACGAGATT -3', *nos* reverse CGGAGCACTCCCGTAGGACAT, *osk* forward 5'- TTGCTGAGCCACGCCCAGAA -3', *osk* reverse 5'- ACATTGGGAATGGTCAGCAGGAAATC -3', *rp49* forward 5'- GCTAAGCTGTCGCACAAA, *rp49* reverse 5'- TCCGGTGGGCAGCATGTG -3'. *rp49* RNA was used as the reference. Data analysis was conducted by using the CFX Manager Software (BioRad) and Microsoft Excel.

smFISH, image analysis, and computational modeling

smFISH was carried out as previously described using published *nos* probe sequences [57, 58, 70]. In summary, ovaries were dissected from yeast-fed females in cold PBS in under 10 minutes and tissues were fixed for 30 minutes in 4% paraformaldehyde and

PBS solution. Tissue was incubated with smFISH probes overnight at 37 ºC in the hybridization solution previously described [57]. For imaging, egg chambers were mounted in Prolong Glass (Life Technologies) and were allowed to cure for 72 hours at room temperature [57, 58]. A Leica STELLARIS 5 confocal microscope was used for imaging *nos* smFISH experiments that are describe in detail [58]. The identification and quantification of unlocalized single *nos* transcripts and localized *nos* homotypic clusters were carried out using a custom MATLAB (Mathworks) program that has been previously described and published [57, 58]. Confocal images shown in Figure 3 are maximum projections that were filtered by a balanced circular difference-of-Gaussian with a center radius size of 1.2 pixels and surround size of 2.2 pixels as previously done for other germ plasm studies [56, 58]. The total number of homotypic clusters identified are reported in the figure legends. For modeling experiments, we employed a previously published model that simulates the formation of germ granules, including *nos* homotypic clusters [58]. The only modeling parameters that were adjusted were 1) carrying capacity, which is regulated by Osk levels, was set from 1 (wild type) to 0.56, and 2) the pool of *nos* transcript expression was set from 1 (wild type) to 0.61 to mimic the RT-PCR levels reported in our results section [58].

Statistical Analysis

Reported p-values between average *nos* homotypic cluster sizes were performed using ANOVA test with a post-hoc Tukey test that was calculated using R statistical programming and R Studio using the function aov and TukeyHSD functions [71, 72]. Violin plots were created using the ggplot and ggstatsplot packages [73, 74].

Acknowledgments

We thank the members of the Gao Lab for discussing and revising this manuscript. We thank Dr. Olivia Rissland and Dr. Akira Nakamura for their kind gifts of antibodies. We thank the Center for Biological Imaging at Kean University for assisting with image acquisition and the members and the Niepielko Lab for their helpful comments and fruitful discussions. Research reported in this publication was supported by the Eunice Kennedy Shriver National Institute of Child Health & Human Development of the National Institutes of Health under award no. R15HD102960 to MGN and 1R15HD092925-01A1 to MG.

Author Contributions

MG conceived and directed the project. MG and MGN wrote the manuscript with input from all authors. EK, MP, IF, and NM performed the fertility assays. AM, CD, and JE generated the CRISPR strains. MGN, DAD, and BMO performed the microscopic analysis, smFISH experiments, and modeling. KS and YM performed the confocal microscopy experiments. BP, ARM, and DG performed the Western blots and data analysis. All authors discussed the results and commented on the manuscript.

Competing Interests

The authors declare no competing interests.

Data Availability

All the data presented in this study are included in this manuscript or its supplementary information.

References

566 1. Nakamura, A., Amikura, R., Hanyu, K. & Kobayashi, S. (2001) Me31B silences
567 translation of oocyte-localizing RNAs through the formation of cytoplasmic RNP
568 complex during Drosophila oogenesis, *Development.* **128**, 3233-42.
569 2. Wang, M., Ly, M., Lugowski, A., Laver, J. D., Lipshitz, H. D., Smibert, C. A. &
570 Rissland, O. S. (2017) ME31B globally represses maternal mRNAs by two distinct
571 mechanisms during the Drosophila maternal-to-zygotic transition, *Elife.* **6**.
572 3. Gotze, M., Dufourt, J., Ihling, C., Rammelt, C., Pierson, S., Sambrani, N., Temme,
573 C., Sinz, A., Simonelig, M. & Wahle, E. (2017) Translational repression of the
574 Drosophila nanos mRNA involves the RNA helicase Belle and RNA coating by Me31B
575 and Trailer hitch, *RNA*.
576 4. Kugler, J. M., Chicoine, J. & Lasko, P. (2009) Bicaudal-C associates with a Trailer
577 Hitch/Me31B complex and is required for efficient Gurken secretion, *Dev Biol.* **328**, 160-
578 72.
579 5. Liu, L., Qi, H., Wang, J. & Lin, H. (2011) PAPI, a novel TUDOR-domain protein,
580 complexes with AGO3, ME31B and TRAL in the nuage to silence transposition,
581 *Development.* **138**, 1863-73.
582 6. Langerak, S., Trombley, A., Patterson, J. R., Leroux, D., Couch, A., Wood, M. P. &
583 Schisa, J. A. (2019) Remodeling of the endoplasmic reticulum in Caenorhabditis
584 elegans oocytes is regulated by CGH-1, *Genesis.* **57**, e23267.
585 7. Ko, S., Kawasaki, I. & Shim, Y. H. (2013) PAB-1, a Caenorhabditis elegans poly(A)-
586 binding protein, regulates mRNA metabolism in germline by interacting with CGH-1 and
587 CAR-1, *PLoS One.* **8**, e84798.

588 8. Kashima, M., Kumagai, N., Agata, K. & Shibata, N. (2016) Heterogeneity of
589 chromatoid bodies in adult pluripotent stem cells of planarian Dugesia japonica, *Dev*
590 *Growth Differ.* **58**, 225-37.
591 9. Yoshida-Kashikawa, M., Shibata, N., Takechi, K. & Agata, K. (2007) DjCBC-1, a
592 conserved DEAD box RNA helicase of the RCK/p54/Me31B family, is a component of
593 RNA-protein complexes in planarian stem cells and neurons, *Dev Dyn.* **236**, 3436-50.
594 10. Alves-Rodrigues, I., Mas, A. & Diez, J. (2007) Xenopus Xp54 and human RCK/p54
595 helicases functionally replace yeast Dhh1p in brome mosaic virus RNA replication, *J*
596 *Virol.* **81**, 4378-80.
597 11. Smillie, D. A. & Sommerville, J. (2002) RNA helicase p54 (DDX6) is a shuttling
598 protein involved in nuclear assembly of stored mRNP particles, *J Cell Sci.* **115**, 395-407.
599 12. Aravin, A. A., van der Heijden, G. W., Castaneda, J., Vagin, V. V., Hannon, G. J. &
600 Bortvin, A. (2009) Cytoplasmic compartmentalization of the fetal piRNA pathway in
601 mice, *PLoS Genet.* **5**, e1000764.
602 13. Swetloff, A., Conne, B., Huarte, J., Pitetti, J. L., Nef, S. & Vassalli, J. D. (2009)
603 Dcp1-bodies in mouse oocytes, *Mol Biol Cell.* **20**, 4951-61.
604 14. Lin, F., Wang, R., Shen, J. J., Wang, X., Gao, P., Dong, K. & Zhang, H. Z. (2008)
605 Knockdown of RCK/p54 expression by RNAi inhibits proliferation of human colorectal
606 cancer cells in vitro and in vivo, *Cancer Biol Ther.* **7**, 1669-76.
607 15. Marcon, B. H., Rebelatto, C. K., Cofre, A. R., Dallagiovanna, B. & Correa, A. (2020)
608 DDX6 Helicase Behavior and Protein Partners in Human Adipose Tissue-Derived Stem
609 Cells during Early Adipogenesis and Osteogenesis, *Int J Mol Sci.* **21**.

610 16. Wang, Y., Arribas-Layton, M., Chen, Y., Lykke-Andersen, J. & Sen, G. L. (2015)
611 DDX6 Orchestrates Mammalian Progenitor Function through the mRNA Degradation
612 and Translation Pathways, *Mol Cell.* **60**, 118-30.
613 17. Hansen, M., Zeddies, S., Meinders, M., di Summa, F., van Alphen, F. P. J.,
614 Hoogendijk, A. J., Moore, K. S., Halbach, M., Gutierrez, L., van den Biggelaar, M.,
615 Thijssen-Timmer, D. C., Auburger, G. W. J., van den Akker, E., von Lindern, M. &
616 Rollmann, E. (2020) The RNA-Binding Protein ATXN2 is Expressed during
617 Megakaryopoiesis and May Control Timing of Gene Expression, *Int J Mol Sci.* **21**.
618 18. Di Stefano, B., Luo, E. C., Haggerty, C., Aigner, S., Charlton, J., Brumbaugh, J., Ji,
619 F., Rabano Jimenez, I., Clowers, K. J., Huebner, A. J., Clement, K., Lipchina, I., de Kort,
620 M. A. C., Anselmo, A., Pulice, J., Gerli, M. F. M., Gu, H., Gygi, S. P., Sadreyev, R. I.,
621 Meissner, A., Yeo, G. W. & Hochedlinger, K. (2019) The RNA Helicase DDX6 Controls
622 Cellular Plasticity by Modulating P-Body Homeostasis, *Cell Stem Cell.* **25**, 622-638 e13.
623 19. Weston, A. & Sommerville, J. (2006) Xp54 and related (DDX6-like) RNA helicases:
624 roles in messenger RNP assembly, translation regulation and RNA degradation, *Nucleic*
625 *Acids Res.* **34**, 3082-94.
626 20. Chu, C. Y. & Rana, T. M. (2006) Translation repression in human cells by
627 microRNA-induced gene silencing requires RCK/p54, *PLoS Biol.* **4**, e210.
628 21. Barckmann, B., Pierson, S., Dufourt, J., Papin, C., Armenise, C., Port, F.,
629 Grentzinger, T., Chambeyron, S., Baronian, G., Desvignes, J. P., Curk, T. & Simonelig,
630 M. (2015) Aubergine iCLIP Reveals piRNA-Dependent Decay of mRNAs Involved in
631 Germ Cell Development in the Early Embryo, *Cell Rep.* **12**, 1205-16.

632 22. Jeske, M., Moritz, B., Anders, A. & Wahle, E. (2011) Smaug assembles an ATP-
633 dependent stable complex repressing nanos mRNA translation at multiple levels, *EMBO*
634 *J.* **30**, 90-103.
635 23. Sudhakaran, I. P., Hillebrand, J., Dervan, A., Das, S., Holohan, E. E., Hulsmeier, J.,
636 Sarov, M., Parker, R., VijayRaghavan, K. & Ramaswami, M. (2014) FMRP and Ataxin-2
637 function together in long-term olfactory habituation and neuronal translational control,
638 *Proc Natl Acad Sci U S A.* **111**, E99-E108.
639 24. DeHaan, H., McCambridge, A., Armstrong, B., Cruse, C., Solanki, D., Trinidad, J.
640 C., Arkov, A. L. & Gao, M. (2017) An in vivo Proteomic Analysis of the Me31B
641 Interactome in Drosophila Germ Granules, *FEBS Lett*.
642 25. Arkov, A. L. & Ramos, A. (2010) Building RNA-protein granules: insight from the
643 germline, *Trends Cell Biol.* **20**, 482-90.
644 26. Voronina, E., Seydoux, G., Sassone-Corsi, P. & Nagamori, I. (2011) RNA granules
645 in germ cells, *Cold Spring Harb Perspect Biol.* **3**.
646 27. Rangan, P., DeGennaro, M., Jaime-Bustamante, K., Coux, R. X., Martinho, R. G. &
647 Lehmann, R. (2009) Temporal and spatial control of germ-plasm RNAs, *Curr Biol.* **19**,
648 72-7.
649 28. McCambridge, A., Solanki, D., Olchawa, N., Govani, N., Trinidad, J. C. & Gao, M.
650 (2020) Comparative Proteomics Reveal Me31B's Interactome Dynamics, Expression
651 Regulation, and Assembly Mechanism into Germ Granules during Drosophila Germline
652 Development, *Sci Rep.* **10**, 564.
653 29. Sankaranarayanan, M., Emenecker, R. J., Jahnel, M., Trussina, I. R. E. A.,
654 Wayland, M., Alberti, S., Holehouse, A. S. & Weil, T. T. (2021) The arrested state of

655 processing bodies supports mRNA regulation in early development, *bioRxiv*,
656 2021.03.16.435709.
657 30. Minshall, N., Kress, M., Weil, D. & Standart, N. (2009) Role of p54 RNA helicase
658 activity and its C-terminal domain in translational repression, P-body localization and
659 assembly, *Mol Biol Cell.* **20**, 2464-72.
660 31. Barbee, S. A., Estes, P. S., Cziko, A. M., Hillebrand, J., Luedeman, R. A., Coller, J.
661 M., Johnson, N., Howlett, I. C., Geng, C., Ueda, R., Brand, A. H., Newbury, S. F.,
662 Wilhelm, J. E., Levine, R. B., Nakamura, A., Parker, R. & Ramaswami, M. (2006)
663 Staufen- and FMRP-containing neuronal RNPs are structurally and functionally related
664 to somatic P bodies, *Neuron.* **52**, 997-1009.
665 32. Minshall, N., Thom, G. & Standart, N. (2001) A conserved role of a DEAD box
666 helicase in mRNA masking, *RNA.* **7**, 1728-42.
667 33. Tritschler, F., Eulalio, A., Helms, S., Schmidt, S., Coles, M., Weichenrieder, O.,
668 Izaurralde, E. & Truffault, V. (2008) Similar modes of interaction enable Trailer Hitch
669 and EDC3 to associate with DCP1 and Me31B in distinct protein complexes, *Mol Cell*
670 *Biol.* **28**, 6695-708.
671 34. Tritschler, F., Braun, J. E., Eulalio, A., Truffault, V., Izaurralde, E. & Weichenrieder,
672 O. (2009) Structural basis for the mutually exclusive anchoring of P body components
673 EDC3 and Tral to the DEAD box protein DDX6/Me31B, *Mol Cell.* **33**, 661-8.
674 35. Peter, D., Ruscica, V., Bawankar, P., Weber, R., Helms, S., Valkov, E., Igreja, C. &
675 Izaurralde, E. (2019) Molecular basis for GIGYF-Me31B complex assembly in 4EHP-
676 mediated translational repression, *Genes Dev.* **33**, 1355-1360.

677 36. Hara, M., Lourido, S., Petrova, B., Lou, H. J., Von Stetina, J. R., Kashevsky, H.,
678 Turk, B. E. & Orr-Weaver, T. L. (2018) Identification of PNG kinase substrates uncovers
679 interactions with the translational repressor TRAL in the oocyte-to-embryo transition,
680 *Elife.* **7**.
681 37. Cheng, Z., Coller, J., Parker, R. & Song, H. (2005) Crystal structure and functional
682 analysis of DEAD-box protein Dhh1p, *RNA.* **11**, 1258-70.
683 38. Intile, P. J., Balzer, G. J., Wolfgang, M. C. & Yahr, T. L. (2015) The RNA Helicase
684 DeaD Stimulates ExsA Translation To Promote Expression of the Pseudomonas
685 aeruginosa Type III Secretion System, *J Bacteriol.* **197**, 2664-74.
686 39. Liao, S. E., Kandasamy, S. K., Zhu, L. & Fukunaga, R. (2019) DEAD-box RNA
687 helicase Belle posttranscriptionally promotes gene expression in an ATPase activity-
688 dependent manner, *RNA.* **25**, 825-839.
689 40. Mugler, C. F., Hondele, M., Heinrich, S., Sachdev, R., Vallotton, P., Koek, A. Y.,
690 Chan, L. Y. & Weis, K. (2016) ATPase activity of the DEAD-box protein Dhh1 controls
691 processing body formation, *Elife.* **5**.
692 41. Story, R. M., Li, H. & Abelson, J. N. (2001) Crystal structure of a DEAD box protein
693 from the hyperthermophile Methanococcus jannaschii, *Proc Natl Acad Sci U S A.* **98**,
694 1465-70.
695 42. Buszczak, M. & Cooley, L. (2000) Eggs to die for: cell death during Drosophila
696 oogenesis, *Cell Death Differ.* **7**, 1071-4.
697 43. McCall, K. & Steller, H. (1998) Requirement for DCP-1 caspase during Drosophila
698 oogenesis, *Science.* **279**, 230-4.

699 44. Shen, R., Weng, C., Yu, J. & Xie, T. (2009) eIF4A controls germline stem cell self-
700 renewal by directly inhibiting BAM function in the Drosophila ovary, *Proc Natl Acad Sci*
701 *U S A.* **106**, 11623-8.
702 45. Oberer, M., Marintchev, A. & Wagner, G. (2005) Structural basis for the
703 enhancement of eIF4A helicase activity by eIF4G, *Genes Dev.* **19**, 2212-23.
704 46. Pause, A., Methot, N. & Sonenberg, N. (1993) The HRIGRXXR region of the DEAD
705 box RNA helicase eukaryotic translation initiation factor 4A is required for RNA binding
706 and ATP hydrolysis, *Mol Cell Biol.* **13**, 6789-98.
707 47. Pause, A. & Sonenberg, N. (1992) Mutational analysis of a DEAD box RNA
708 helicase: the mammalian translation initiation factor eIF-4A, *EMBO J.* **11**, 2643-54.
709 48. Pause, A., Methot, N., Svitkin, Y., Merrick, W. C. & Sonenberg, N. (1994) Dominant
710 negative mutants of mammalian translation initiation factor eIF-4A define a critical role
711 for eIF-4F in cap-dependent and cap-independent initiation of translation, *EMBO J.* **13**,
712 1205-15.
713 49. Chen, W., Hu, Y., Lang, C. F., Brown, J. S., Schwabach, S., Song, X., Zhang, Y.,
714 Munro, E., Bennett, K., Zhang, D. & Lee, H. C. (2020) The Dynamics of P Granule
715 Liquid Droplets Are Regulated by the Caenorhabditis elegans Germline RNA Helicase
716 GLH-1 via Its ATP Hydrolysis Cycle, *Genetics.* **215**, 421-434.
717 50. Marnik, E. A., Fuqua, J. H., Sharp, C. S., Rochester, J. D., Xu, E. L., Holbrook, S.
718 E. & Updike, D. L. (2019) Germline Maintenance Through the Multifaceted Activities of
719 GLH/Vasa in Caenorhabditis elegans P Granules, *Genetics.* **213**, 923-939.
720 51. Lehmann, R. (2016) Germ Plasm Biogenesis--An Oskar-Centric Perspective, *Curr*
721 *Top Dev Biol.* **116**, 679-707.

722 52. Gao, M. & Arkov, A. L. (2013) Next generation organelles: structure and role of
723 germ granules in the germline, *Mol Reprod Dev.* **80**, 610-23.
724 53. Jamieson-Lucy, A. & Mullins, M. C. (2019) The vertebrate Balbiani body, germ
725 plasm, and oocyte polarity, *Curr Top Dev Biol.* **135**, 1-34.
726 54. Bilinski, S. M., Jaglarz, M. K. & Tworzydlo, W. (2017) The Pole (Germ) Plasm in
727 Insect Oocytes, *Results Probl Cell Differ.* **63**, 103-126.
728 55. Wang, J. T. & Seydoux, G. (2013) Germ cell specification, *Adv Exp Med Biol.* **757**,
729 17-39.
730 56. Little, S. C., Sinsimer, K. S., Lee, J. J., Wieschaus, E. F. & Gavis, E. R. (2015)
731 Independent and coordinate trafficking of single Drosophila germ plasm mRNAs, *Nat*
732 *Cell Biol.* **17**, 558-68.
733 57. Niepielko, M. G., Eagle, W. V. I. & Gavis, E. R. (2018) Stochastic Seeding Coupled
734 with mRNA Self-Recruitment Generates Heterogeneous Drosophila Germ Granules,
735 *Curr Biol.* **28**, 1872-1881 e3.
736 58. Valentino, M., Ortega, B. M., Ulrich, B., Doyle, D. A., Farnum, E. D., Joiner, D. A.,
737 Gavis, E. R. & Niepielko, M. G. (2022) Computational modeling offers new insight into
738 Drosophila germ granule development, *Biophys J.* **121**, 1465-1482.
739 59. Huang, J. H., Ku, W. C., Chen, Y. C., Chang, Y. L. & Chu, C. Y. (2017) Dual
740 mechanisms regulate the nucleocytoplasmic localization of human DDX6, *Sci Rep.* **7**,
741 42853.
742 60. Mossman, J. A., Mabeza, R. M. S., Blake, E., Mehta, N. & Rand, D. M. (2019) Age
743 of Both Parents Influences Reproduction and Egg Dumping Behavior in Drosophila
744 melanogaster, *J Hered.* **110**, 300-309.

745 61. Tritschler, F., Eulalio, A., Truffault, V., Hartmann, M. D., Helms, S., Schmidt, S.,
746 Coles, M., Izaurralde, E. & Weichenrieder, O. (2007) A divergent Sm fold in EDC3
747 proteins mediates DCP1 binding and P-body targeting, *Mol Cell Biol.* **27**, 8600-11.
748 62. Sankaranarayanan, M., Emenecker, R. J., Wilby, E. L., Jahnel, M., Trussina, I.,
749 Wayland, M., Alberti, S., Holehouse, A. S. & Weil, T. T. (2021) Adaptable P body
750 physical states differentially regulate bicoid mRNA storage during early Drosophila
751 development, *Dev Cell.* **56**, 2886-2901 e6.
752 63. Nguyen Ba, A. N., Pogoutse, A., Provart, N. & Moses, A. M. (2009) NLStradamus:
753 a simple Hidden Markov Model for nuclear localization signal prediction, *BMC*
754 *Bioinformatics.* **10**, 202.
755 64. Kosugi, S., Hasebe, M., Tomita, M. & Yanagawa, H. (2009) Systematic
756 identification of cell cycle-dependent yeast nucleocytoplasmic shuttling proteins by
757 prediction of composite motifs, *Proc Natl Acad Sci U S A.* **106**, 10171-6.
758 65. Lin, J. R. & Hu, J. (2013) SeqNLS: nuclear localization signal prediction based on
759 frequent pattern mining and linear motif scoring, *PLoS One.* **8**, e76864.
760 66. Gratz, S. J., Ukken, F. P., Rubinstein, C. D., Thiede, G., Donohue, L. K.,
761 Cummings, A. M. & O'Connor-Giles, K. M. (2014) Highly specific and efficient
762 CRISPR/Cas9-catalyzed homology-directed repair in Drosophila, *Genetics.* **196**, 961-
763 71.
764 67. Gratz, S. J., Rubinstein, C. D., Harrison, M. M., Wildonger, J. & O'Connor-Giles, K.
765 M. (2015) CRISPR-Cas9 Genome Editing in Drosophila, *Curr Protoc Mol Biol.* **111**, 31 2
766 1-20.

767 68. Creed, T. M., Loganathan, S. N., Varonin, D., Jackson, C. A. & Arkov, A. L. (2010)
768 Novel role of specific Tudor domains in Tudor-Aubergine protein complex assembly and
769 distribution during Drosophila oogenesis, *Biochem Biophys Res Commun.* **402**, 384-9.
770 69. Arkov, A. L., Wang, J. Y., Ramos, A. & Lehmann, R. (2006) The role of Tudor
771 domains in germline development and polar granule architecture, *Development.* **133**,
772 4053-62.
773 70. Eagle, W. V. I., Yeboah-Kordieh, D. K., Niepielko, M. G. & Gavis, E. R. (2018)
774 Distinct cis-acting elements mediate targeting and clustering of Drosophila polar granule
775 mRNAs, *Development.* **145**.
776 71. Team, R. (2020) RStudio: Integrated Development Environment for R in, RStudio,
777 PBC., Boston, MA.
778 72. Team, R. C. (2020) R: A Language and Environment for Statistical Computing in, R
779 Foundation for Statistical Computing,
780 73. Wickham, H. (2016) *ggplot2: Elegant Graphics for Data Analysis*, pringer-Verlag
781 New York.
782 74. Patil, I. (2021) Visualizations with statistical details: The ggstatsplot approach,
783 *Journal of Open Source Software.* **6**, 3167.

784

Figure Legends

Figure 1. Diagram of the Me31B wildtype and mutant proteins in the *Drosophila* strains generated in this study. The bar shape after each Me31B protein name represents the primary structure of the protein. The numbers on top of the bars mark the number of amino acids and their positions in the protein. Green Fluorescence Protein (GFP) tags are expressed at the C-terminal end of the constructed Me31B proteins. The point mutations are as follows: E208A, glutamic acid 208 replaced by alanine; R101A, arginine 101 replaced by alanine; K103A, lysine 103 replaced by alanine; R385Q, arginine 385 replaced by glutamine; C285A, cysteine 285 replaced by alanine; L289A, leucine 289 replaced by alanine; Y273S, tyrosine 273 replaced by serine; Y274N, tyrosine 274 replaced by asparagine. Me31B$^{N\text{-}ter}$ protein (deletion of amino acids 277 to 459) contains the first 276 amino acids of the wildtype protein. Me31B$^{C\text{-}ter}$ protein (deletion of amino acids 1 to 276) contains the last 183 amino acids of the wildtype protein.

*Note that two unintended, mis-sense mutations were detected in the *me31B^{FDF}* strain when sequencing its *me31B* gene. The two mutations (Y273S and Y274N) are outside the FDF motif-binding motif.

Figure 2. Defective embryogenesis and oogenesis of heterozygous *me31B^{E208A}*, *me31B^{DVLAAAA}*, and *me31B^{R385Q}* strains. (A) Embryos laid by *w^{1118}* control females all had normal (100%) dorsal appendages. In contrast, embryos laid by *me31B^{E208A}*/+ females had fused (45%), shortened (33%), and normal (22%, not shown) dorsal appendages; embryos laid by *me31B^{DVLAAAA}*/+ females had shortened (33%) or normal (67%, not shown) dorsal appendages; embryos laid by *me31B^{R385Q}*/+ females all had

808 severe morphological defects (100%). **(B)** In 52% of late-stage (stage 14) eggs of
809 *me31B*^{E208A}/+ mutant (right panel), dumping of the nurse cell content into the oocyte
810 was incomplete (see highlighted region with yellow dashed lines), in contrast to the
811 complete dumping of *w*^{1118} control eggs (left panel). DAPI staining of the same eggs
812 was shown at the bottom panels, and nurse cell nuclei-like materials were present in the
813 "un-dumped" region of the *me31B*^{E208A}/+ mutant egg. **(C)** Similar dumpless phenotypes
814 were observed in 78% of *me31B*^{DVLAAAA}/+ mutant's late-stage (stage 14) eggs. The "un-
815 dumped" regions (highlighted with yellow dashed lines) were broader than the
816 *me31B*^{E208A}/+ mutant from (B). Only 22% of *me31B*^{DVLAAAA}/+ mutant's eggs appeared
817 normal. **(D)** Ovarioles from *w*^{1118} and *me31B*^{R385Q}/+ females were stained by DAPI stain.
818 The ovarioles are oriented so that the early-stage egg chambers are on the left and the
819 later-stage egg chambers are on the right. Early-to-mid stage egg chamber
820 degenerations in *me31B*^{R385Q}/+ mutant (right panel) are indicated by arrows, in contrast
821 to the successfully developed early- and mid-stage egg chambers in the *w*^{1118} control
822 (left panel).

823 **Figure 3. smFISH analysis of *nos* mRNA in *me31B*^{DVLAAAA} heterozygous mutant**
824 **and quantitative RT-PCR analysis of *nos* and *osk* mRNA levels in heterozygous**
825 ***me31B*^{E208A}, *me31B*^{DVLAAAA}, and *me31B*^{R385Q} mutants. (A)** Stage 13 oocytes from
826 *me31B*^{WT} and *me31B*^{DVLAAAA} flies, with *nos* (magenta) mRNAs detected using smFISH.
827 The white solid box indicates the unlocalized single transcripts of *nos* that are found in
828 the bulk cytoplasm (enlarged in the second panel) while the broken yellow box
829 highlights *nos* that has localized to the germ plasm by forming homotypic clusters
830 (enlarged and shown as a heatmap in the third panel). **(B)** The distribution of *nos* cluster

size (number of *nos* transcripts calculated within a granule) found in each genotype's germ plasm and the computational model. Total clusters identified and analyzed include 3,295 from *me31B*^{DVLAAA}, 5,551 from the computational model, 19,195 *me31B*^{WT}, and 19,147 from *yellow white* (*yw*). Of note, only oocytes that did not display a dumpless phenotype were included in this analysis. **(C)** In *me31B*^{DVLAAAA}/+ ovaries, *nos* transcript level is 61% ± 7% of that in the *w*^{1118} control ($p < 0.05$) and *osk* transcript level is 56% ± 4% of that in the control ($p < 0.05$). **(D)** In *me31B*^{E208A}/+ ovaries, *nos* transcript level is 104% ± 7% of that in the *w*^{1118} control (NS) and *osk* transcript level is 162% ± 12% of that in the control (NS, $p = 0.054$). (E) In *me31B*^{R285Q}/+ ovaries, *nos* transcript level is 44% ± 2% of that in the *w*^{1118} control ($p < 0.001$) and *osk* transcript level is 194% ± 12% of that in the control ($p < 0.001$). NS, not significant. Error bar represents standard error of the mean.

Figure 4. Fertility assays of *me31B*$^{N\text{-}ter}$, *me31B*$^{C\text{-}ter}$, *me31B*^{FDF} mutants. (A) A *me31B*^{WT} (control), *me31B*$^{N\text{-}ter}$, *me31B*$^{C\text{-}ter}$, and *me31B*^{FDF} female fly laid an average of 117, 68, 29, and 77 eggs, respectively. The egg number of *me31B*$^{N\text{-}ter}$, *me31B*$^{C\text{-}ter}$, and *me31B*^{FDF} mutants are 58% ($p < 0.01$), 25% ($p< 0.001$), and 66% ($p < 0.05$) of the *me31B*^{WT} (control), respectively. **(B)** A *me31B*^{WT} (control), *me31B*$^{N\text{-}ter}$, *me31B*$^{C\text{-}ter}$, and *me31B*^{FDF} female fly produced an average of 106, 47, 0, and 75 progenies, respectively. The progeny number of *me31B*$^{N\text{-}ter}$, *me31B*$^{C\text{-}ter}$ and *me31B*^{FDF} mutants are 44% ($p < 0.001$), 0% ($p < 0.0001$), and 71% (NS) respectively. NS, not significant. **(C)** The average egg hatch rates for *me31B*^{WT} (control), *me31B*$^{N\text{-}ter}$, *me31B*$^{C\text{-}ter}$, and *me31B*^{FDF} strains are 90.8%, 68.3%, 0%, and 97.1%, respectively. Compared to *me31B*^{WT}, the hatch rate decreases in *me31B*$^{N\text{-}ter}$ and *me31B*$^{C\text{-}ter}$ mutants are statistically significant

but not significant in *me31B*^{FDF}. **(D)** Embryos laid by *me31B*$^{C\text{-}ter}$ flies had fused dorsal appendages (68%) or missing dorsal appendages (32%), in contrast to the normal dorsal appendages (100%) in *me31B*^{WT} (control). Error bar represents standard error of the mean.

Figure 5. Western blot quantification of Me31B protein level in *me31B*$^{N\text{-}ter}$, *me31B*$^{C\text{-}ter}$, *me31B*^{FDF} mutants. (A) Anti-GFP Western blots were used to quantify the Me31B^{WT}-GFP, Me31B$^{N\text{-}ter}$-GFP, Me31B$^{C\text{-}ter}$-GFP, and Me31B^{FDF}-GFP proteins in the ovaries of the corresponding fly strains. Anti-Tubulin Western blots were used as loading controls. The expression level of Me31B$^{N\text{-}ter}$ and Me31B$^{C\text{-}ter}$ proteins were conspicuously lower than the Me31B^{WT} control protein, while the Me31B^{FDF} protein level is comparable to the control. The images shown are representative images of multiple biological replicates. The additional, uncropped biological replicate images are presented in Supplementary Figure 2. **(B)** The Me31B$^{N\text{-}ter}$-GFP and Me31B$^{C\text{-}ter}$-GFP protein levels are 40% ($p < 0.01$) and 11% ($p < 0.001$) relative to the Me31B^{WT}-GFP control protein, respectively. Me31B^{FDF}-GFP protein level is 114% relative to the control (NS). Western blot image analysis was performed with ImageJ and protein quantifications were normalized by using the alpha-tubulin proteins. NS, not statistically significant. Error bar represents standard error of the mean.

Figure 6. Mutant Me31B proteins in *me31B*$^{N\text{-}ter}$, *me31B*$^{C\text{-}ter}$, *me31B*^{FDF} strain show altered aggregation and localization in developing egg chambers. (A) In early-stage egg chambers, mutant Me31B-GFP proteins (green channel) in *me31B*$^{N\text{-}ter}$, *me31B*$^{C\text{-}ter}$, and *me31B*^{FDF} strains are much more diffused in the nurse cell and oocytes, in contrast to the aggregated status of Me31B^{WT} in RNP granules like nuage granules

and P-bodies. And none of the three mutant proteins overlap with partner protein Tral. Unlike Me31B mutant proteins, Tral (Red channel) localization are not affected in the three mutants. Particularly, Me31B$^{N\text{-}ter}$-GFP proteins are present in the nuclei of nurse cells. Me31B$^{C\text{-}ter}$-GFP proteins form fewer numbers and smaller size granules than Me31B^{WT}-GFP, and the Me31B$^{C\text{-}ter}$ granules do not associate with Tral-marked granules. Nurse cell perinuclear regions (nuage) are indicated by arrowheads. P-body granules marked by Tral are indicated by arrows. Note that Me31B$^{C\text{-}ter}$-GFP and Me31B^{FDF}-GFP proteins were found in ring-like structures that appear to be ring canals (yellow dashed squares, same for B and C), structures that connect the cytoplasm between nurse cells and oocytes and allow for intracellular transportations. **(B)** In early-to-mid stage egg chambers, mutant Me31B-GFP proteins (green channel) in *me31B$^{N\text{-}ter}$* and *me31B$^{C\text{-}ter}$* strains do not enrich in the developing oocytes like that in the *me31B^{WT}* control. Me31B^{FDF}-GFP protein's enrichment in the developing oocytes is weaker than that in the control. Tral (red channel)'s enrichment in the oocytes is not affected in the three mutants. Developing oocytes are indicated by arrowheads. **(C)** In mid-stage egg chambers, mutant Me31B-GFP proteins of *me31B$^{N\text{-}ter}$*, *me31B$^{C\text{-}ter}$, and me31B^{FDF}* strains localize to the cortex and the germplasm area at the posterior of oocytes, like the control. However, all three mutant Me31B proteins appear more diffused than the aggregated Me31B^{WT}-GFP proteins in the above areas. The germplasm areas are indicated by arrowheads. Tral protein (Red channel)'s localization to the cortex and germplasm was not affected in the three mutants.

Figure 7. Summary of the Me31B motif functions. This study uses a target-motif-mutation approach to investigate six functionally important domains/motifs of *Drosophila*

Me31B. Our characterization of the generated *me31B* mutants revealed ATPase/helicase motifs' function in female fertility, oogenesis, and embryogenesis (DVLARARK, DEAD-box, and HRIGR motifs). An in-depth analysis of the DVLARAK motif mutation uncovered its function in maintaining *nos* mRNA localization and the transcript level of *nos* and *osk* mRNA levels. We further showed the Me31B N-terminal motif, C-terminal motif, and FDF motif-binding motif's function in female fertility and their different roles in maintaining Me31B protein level and subcellular localization.

Figure 1

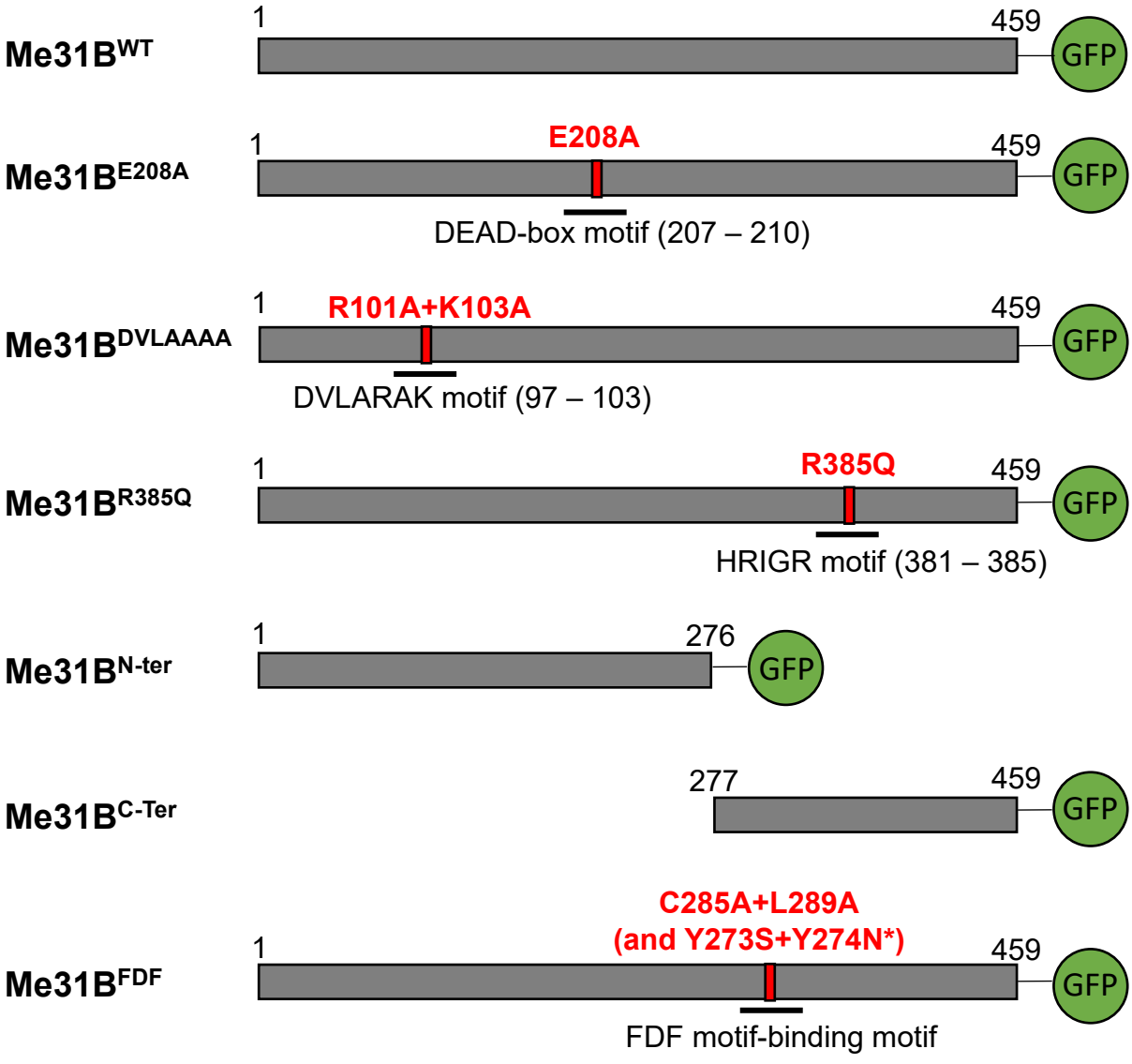
Me31B^WT
1
459
GFP
Me31B^E208A
E208A
1
459
GFP
DEAD-box motif (207 – 210)
Me31B^DVLAAAA
R101A+K103A
1
459
GFP
DVLARAK motif (97 – 103)
Me31B^R385Q
R385Q
1
459
GFP
HRIGR motif (381 – 385)
Me31B^N-ter
1
276
GFP
Me31B^C-Ter
277
459
GFP
Me31B^FDF
C285A+L289A
(and Y273S+Y274N*)
1
459
GFP
FDF motif-binding motif

Figure 2

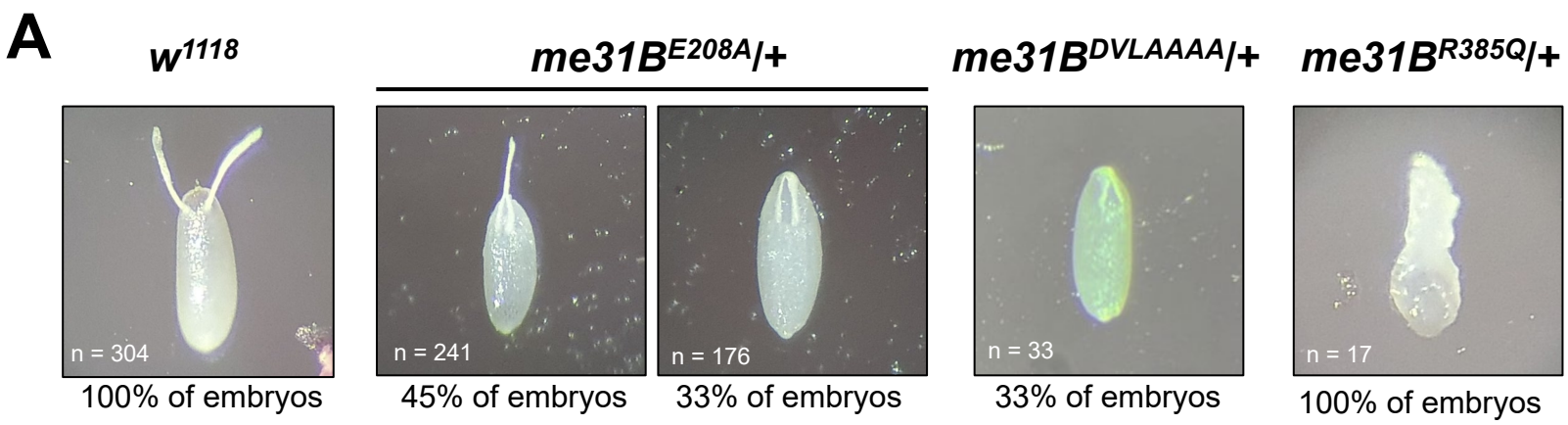

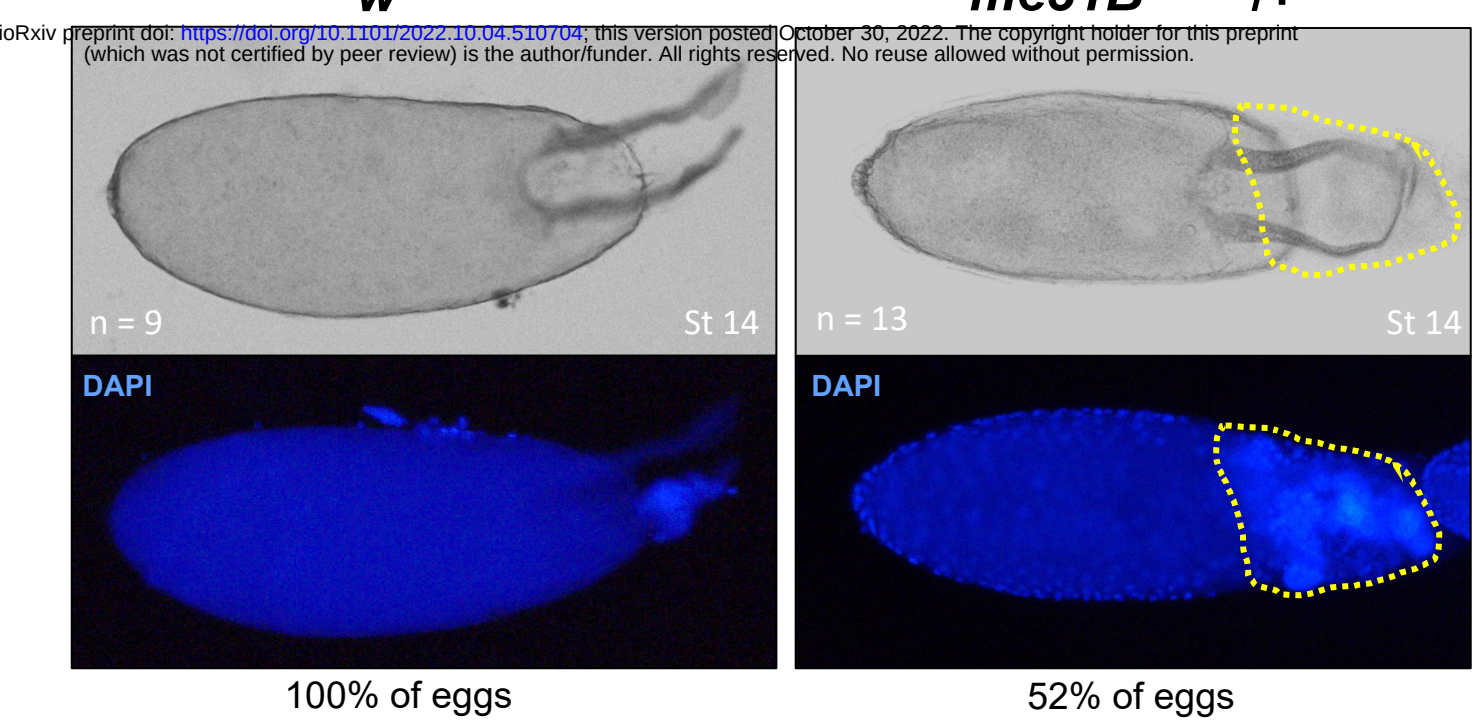

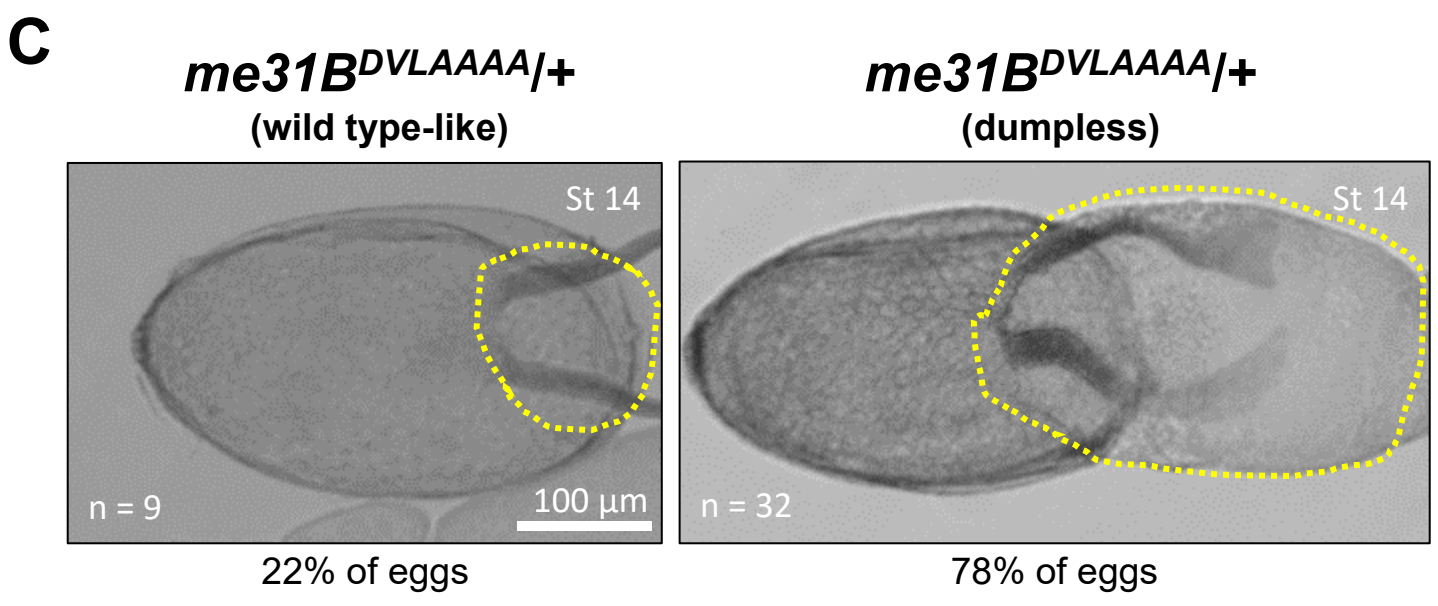

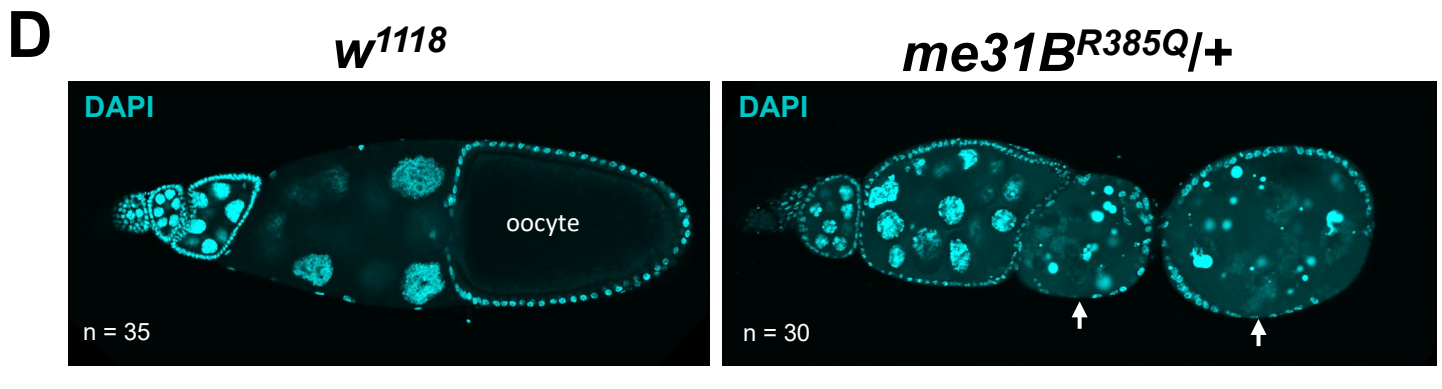

Figure 3

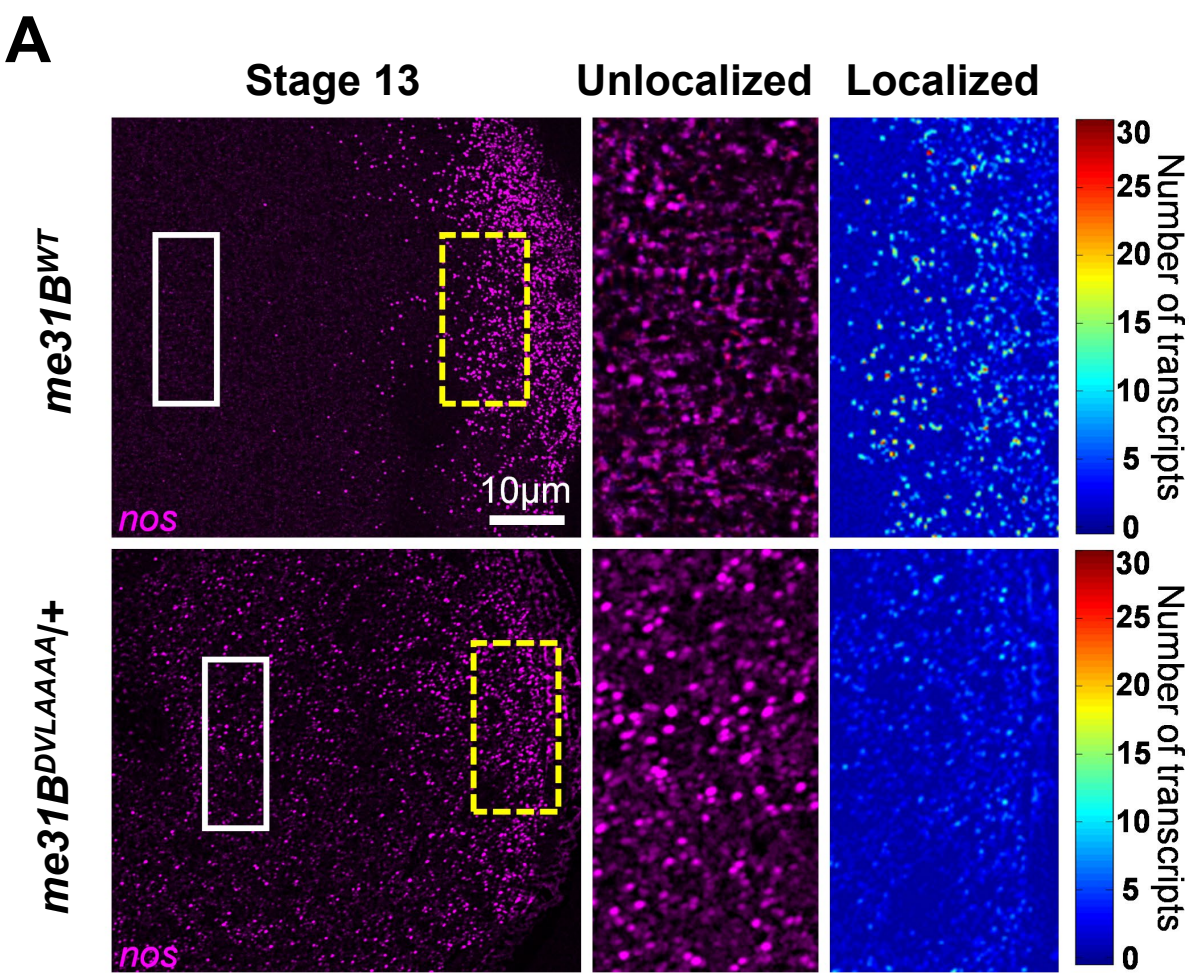

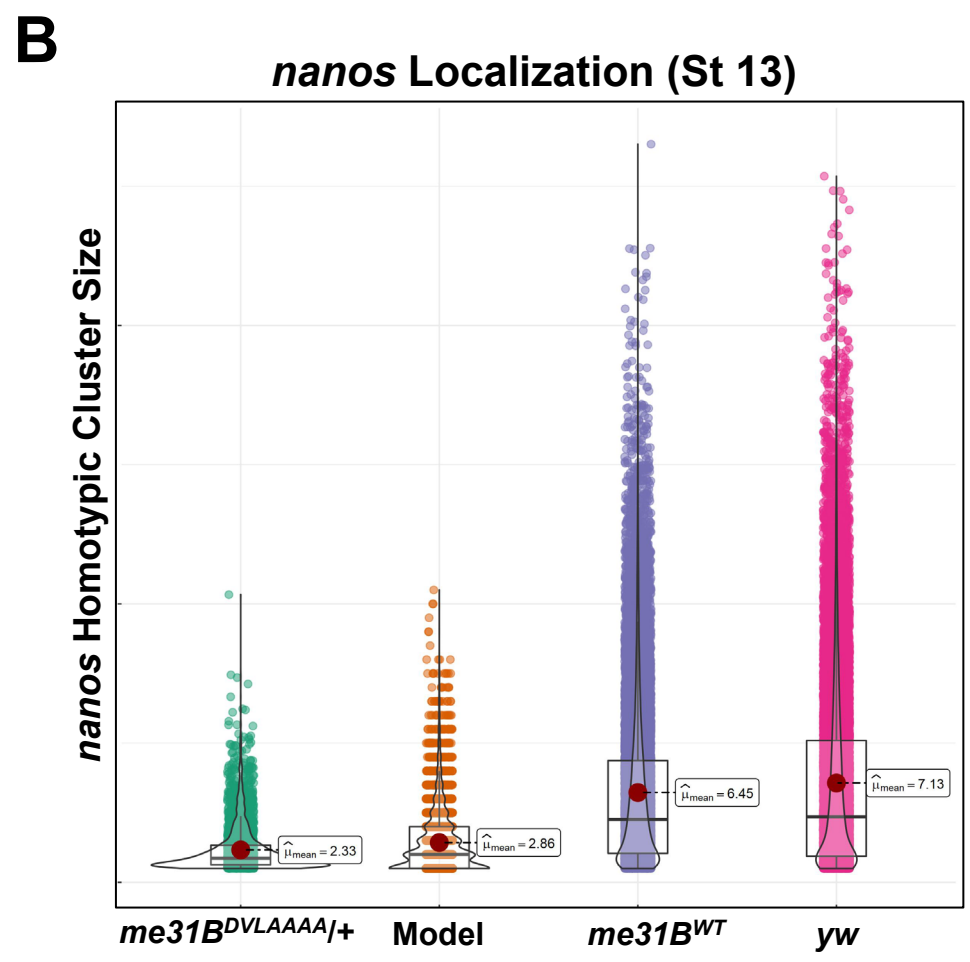

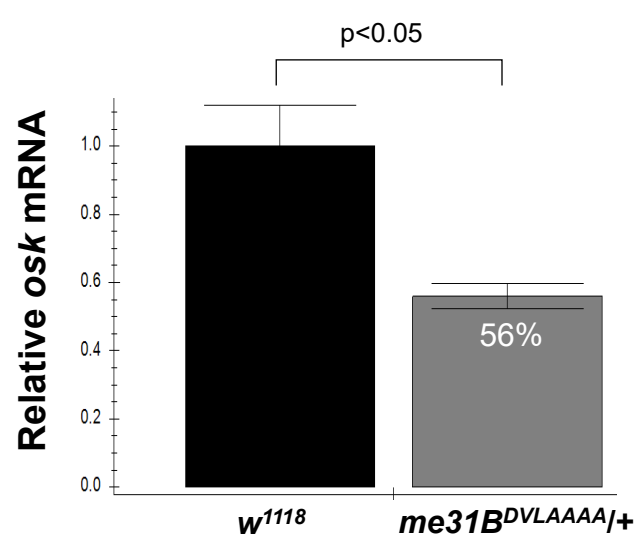

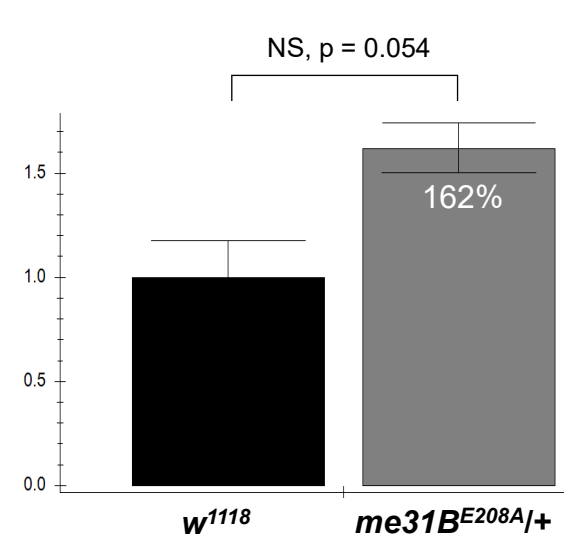

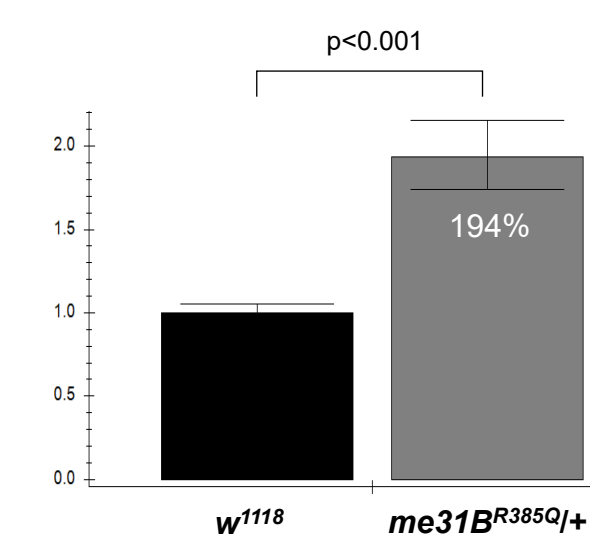

Figure 4

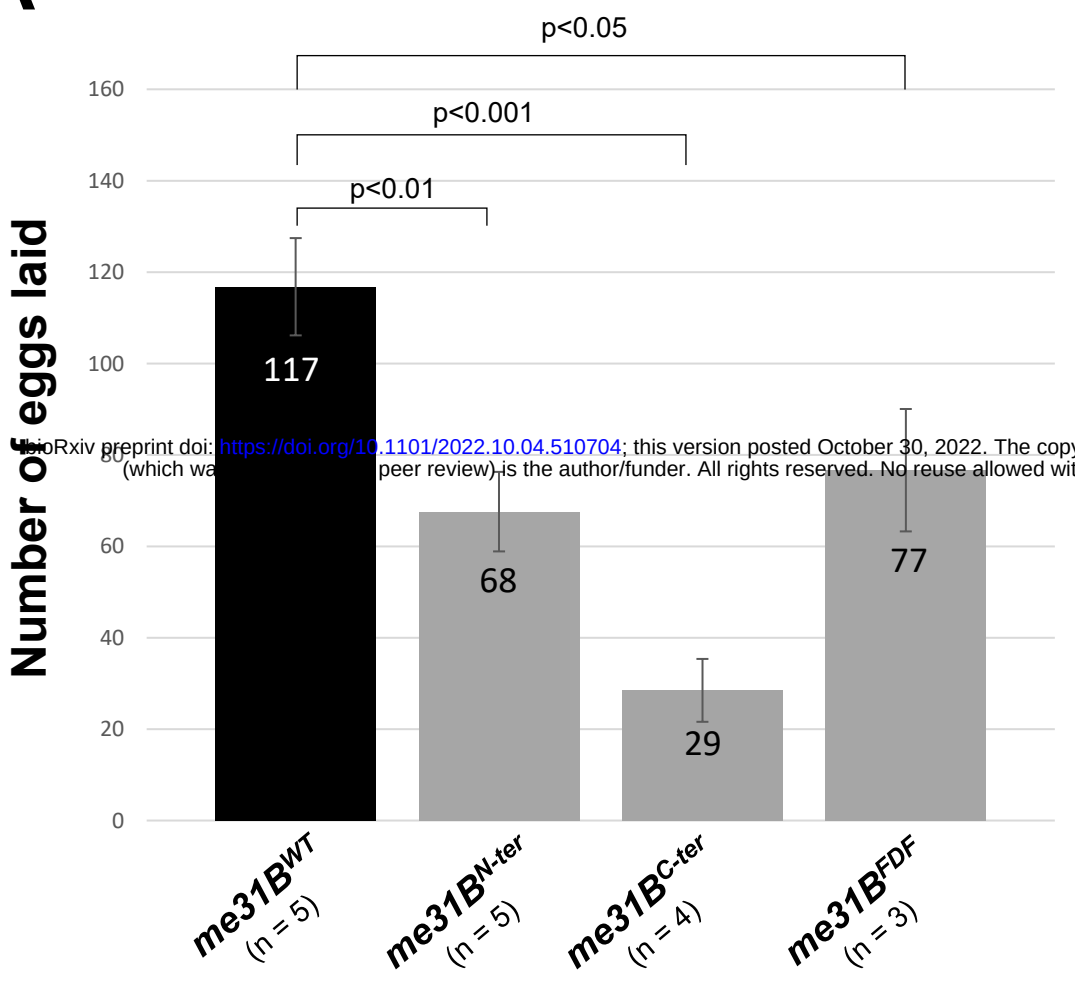

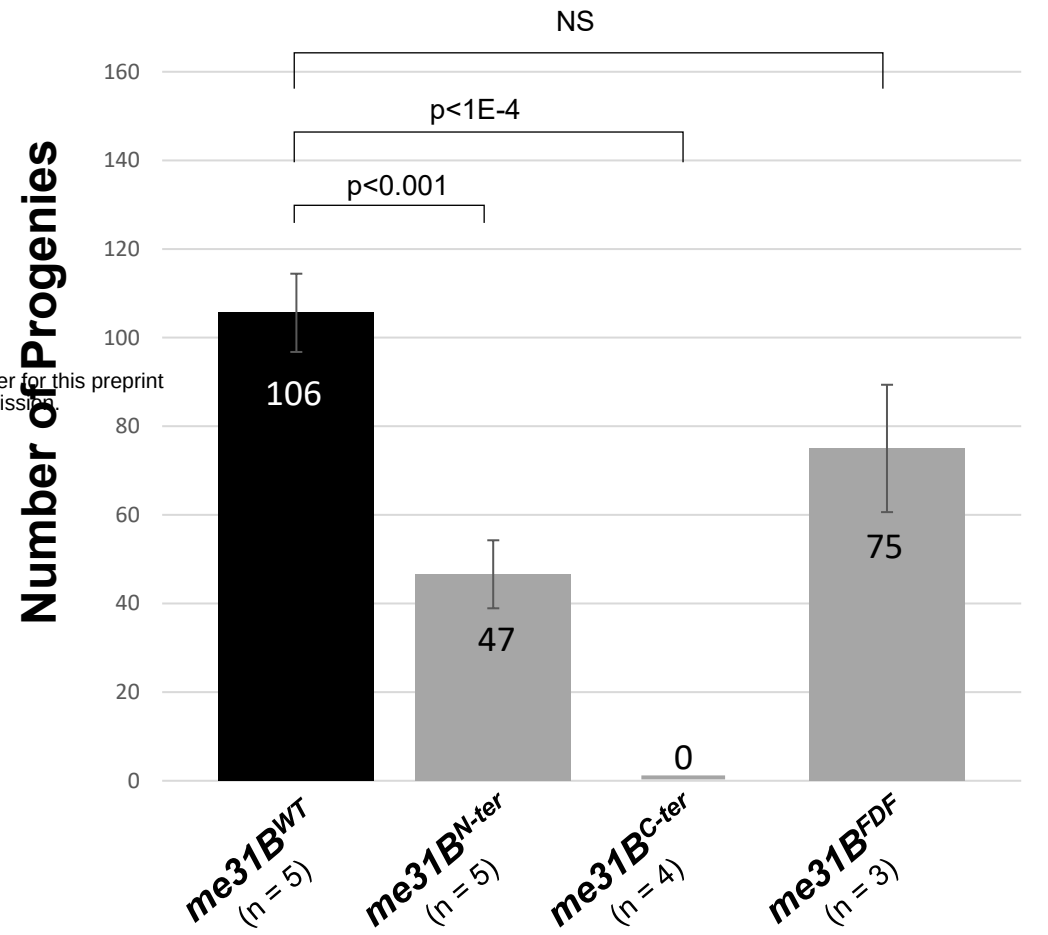

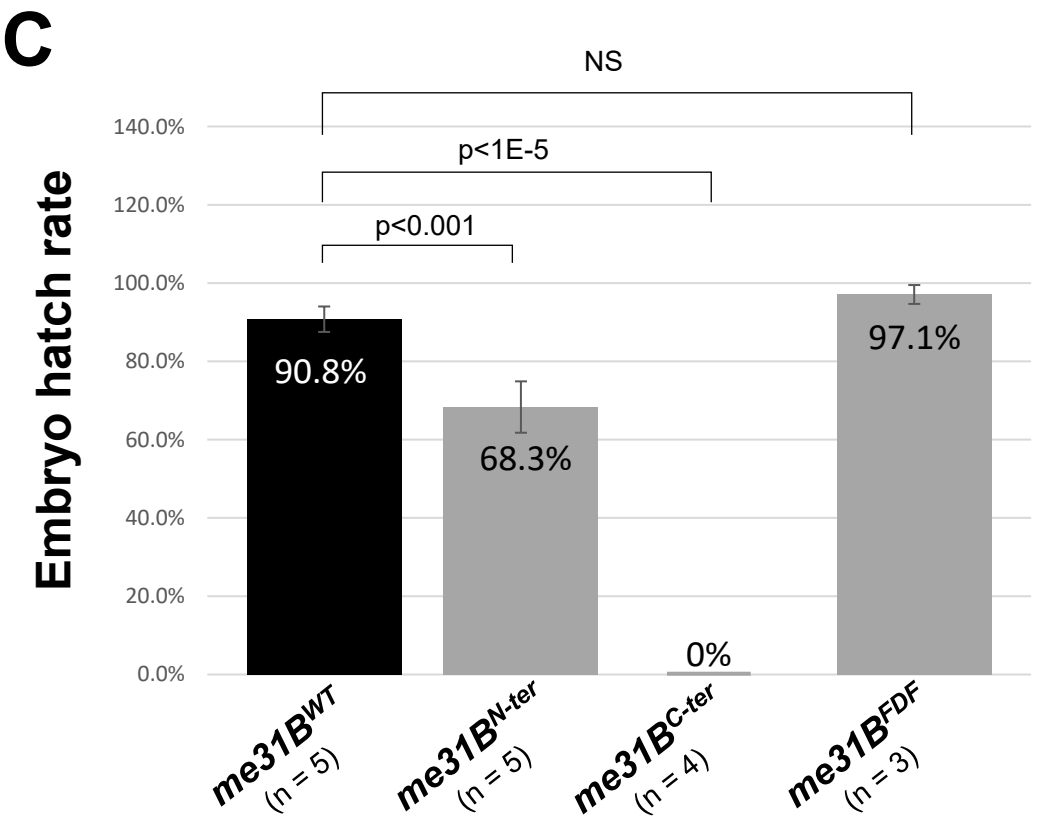

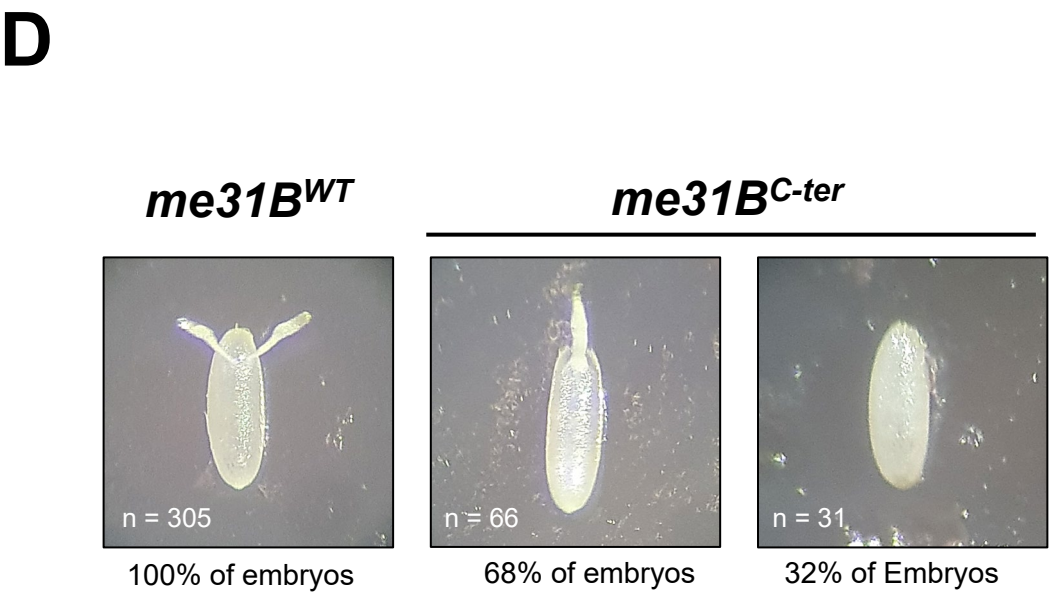

Figure 5

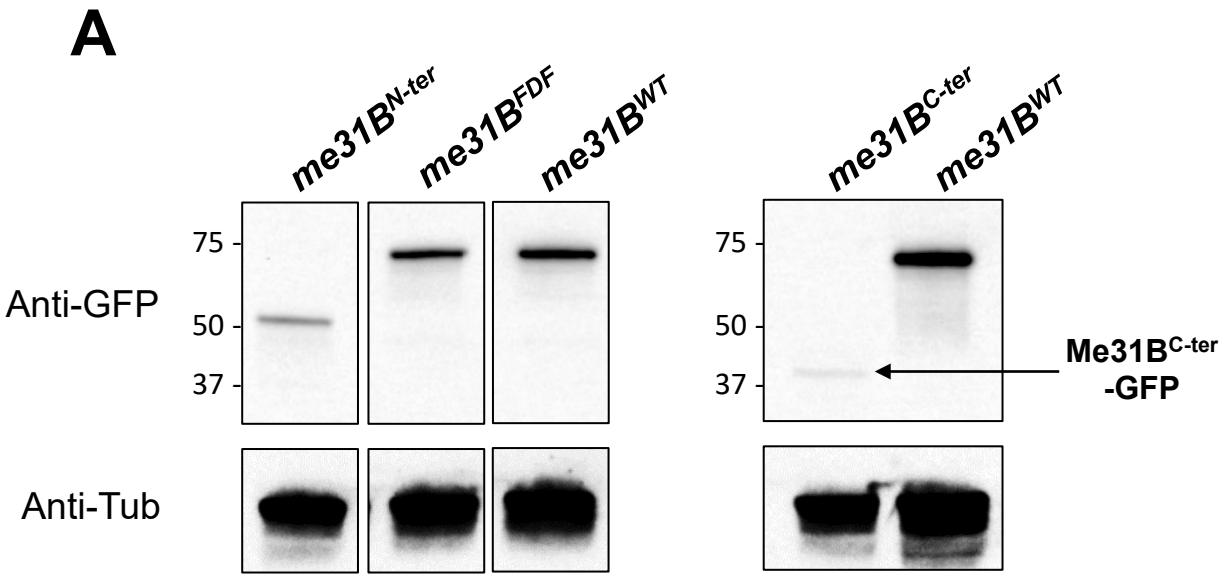
A
me31B^N-ter
me31B^FDF
me31B^WT
me31B^C-ter
me31B^WT
Anti-GFP
Anti-Tub
75
50
37
75
50
37
Me31B^C-ter
-GFP

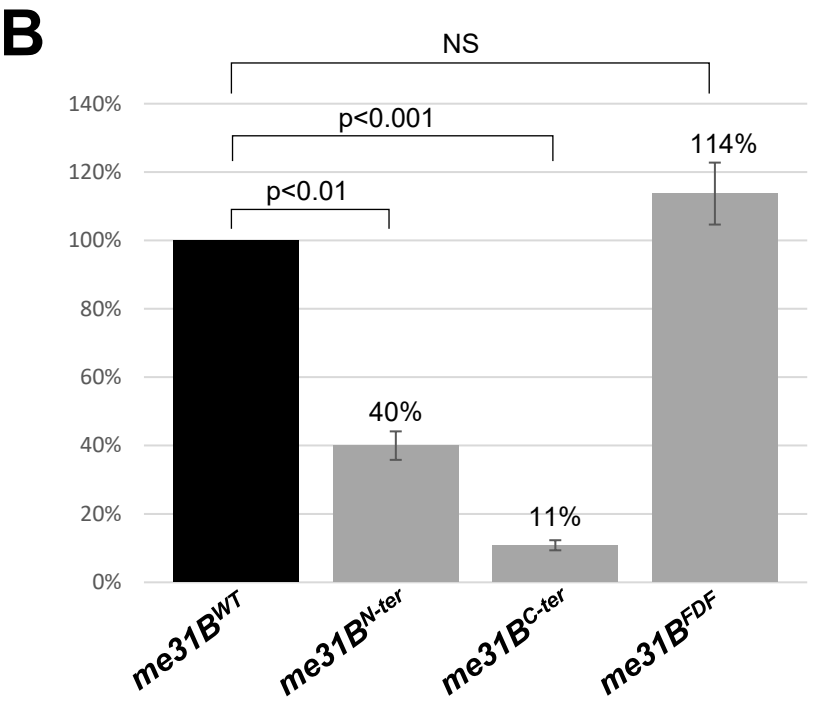
B
NS
p<0.001
p<0.01
114%
40%
11%
140%
120%
100%
80%
60%
40%
20%
0%
me31B^WT
me31B^N-ter
me31B^C-ter
me31B^FDF

Figure 6

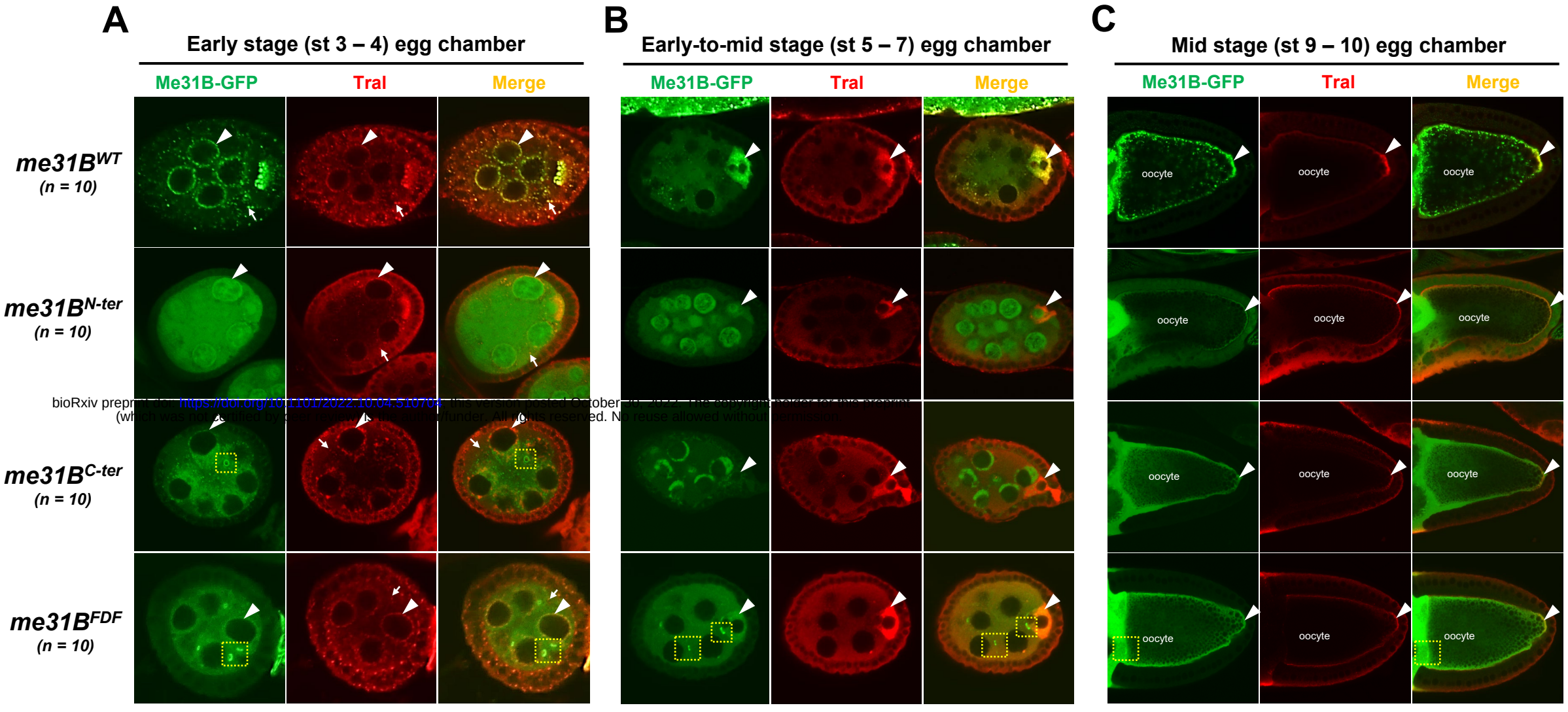

Figure 7

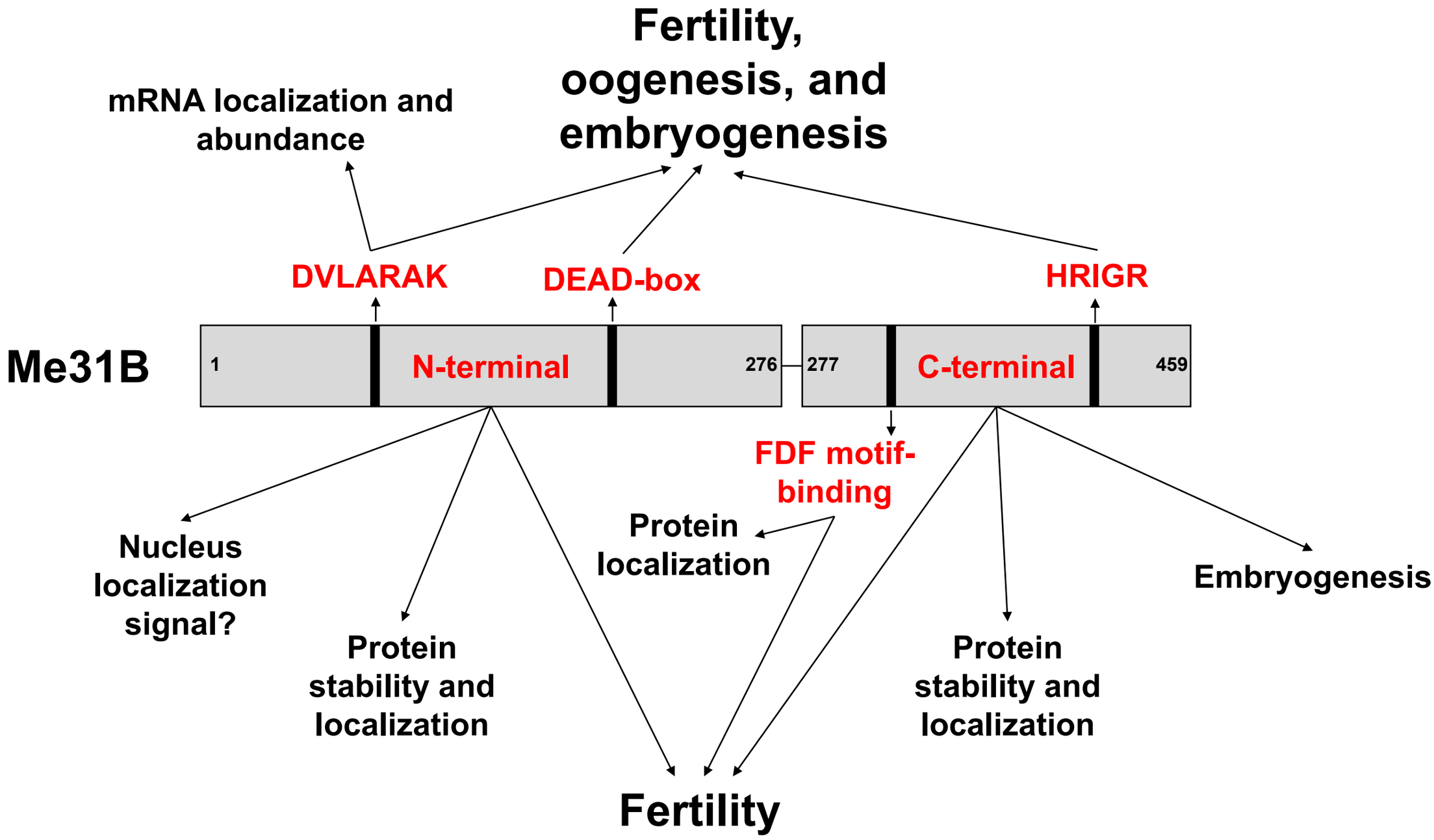
Fertility, oogenesis, and embryogenesis
mRNA localization and abundance
DVLARAK
DEAD-box
HRIGR
Me31B
1
N-terminal
276
277
C-terminal
459
FDF motif-binding
Nucleus localization signal?
Protein stability and localization
Protein localization
Protein stability and localization
Embryogenesis
Fertility